NAVAL POSTGRADUATE SCHOOL

MONTEREY, CALIFORNIA

THESIS

FLUID-STRUCTURE INTERACTION IN A FLUID-FILLED COMPOSITE STRUCTURE SUBJECTED TO LOW VELOCITY IMPACT

by

Taylor J. South

June 2016

Thesis Advisor: Young W. Kwon
Second Reader: Jarema M. Didoszak

Approved for public release; distribution is unlimited

THIS PAGE INTENTIONALLY LEFT BLANK

REPORT DOCUMENTATION PAGE		*Form Approved OMB No. 0704–0188*

Public reporting burden for this collection of information is estimated to average 1 hour per response, including the time for reviewing instruction, searching existing data sources, gathering and maintaining the data needed, and completing and reviewing the collection of information. Send comments regarding this burden estimate or any other aspect of this collection of information, including suggestions for reducing this burden, to Washington headquarters Services, Directorate for Information Operations and Reports, 1215 Jefferson Davis Highway, Suite 1204, Arlington, VA 22202–4302, and to the Office of Management and Budget, Paperwork Reduction Project (0704–0188) Washington DC 20503.

1. AGENCY USE ONLY (*Leave blank*)	2. REPORT DATE June 2016	3. REPORT TYPE AND DATES COVERED Master's thesis	
4. TITLE AND SUBTITLE FLUID-STRUCTURE INTERACTION IN A FLUID-FILLED COMPOSITE STRUCTURE SUBJECTED TO LOW VELOCITY IMPACT		**5. FUNDING NUMBERS**	
6. AUTHOR(S) Taylor J. South			
7. PERFORMING ORGANIZATION NAME(S) AND ADDRESS(ES) Naval Postgraduate School Monterey, CA 93943–5000		**8. PERFORMING ORGANIZATION REPORT NUMBER**	
9. SPONSORING /MONITORING AGENCY NAME(S) AND ADDRESS(ES) N/A		**10. SPONSORING / MONITORING AGENCY REPORT NUMBER**	
11. SUPPLEMENTARY NOTES The views expressed in this thesis are those of the author and do not reflect the official policy or position of the Department of Defense or the U.S. Government. IRB Protocol number ____N/A____.			
12a. DISTRIBUTION / AVAILABILITY STATEMENT Approved for public release; distribution is unlimited		**12b. DISTRIBUTION CODE**	

13. ABSTRACT (maximum 200 words)

   The effects of fluid structure interaction in a fluid-filled cubic composite structure subjected to low velocity impact are the focus of this study. A fabrication technique was developed for creating an E-glass composite cubic structure and a pendulum was designed and built to provide a repeatable low velocity impact. The behavior of the composite structure was studied at various fluid fill levels and impact velocities. The fluid level inside the structure was varied incrementally from empty (0% fill) to full (100% fill). With impact load measurements, strain measurements on each side, and high-speed video, the behavior for each test case was analyzed and compared. Two types of baffles were designed and fabricated out of dense foam material. The behavior of the structure with and without a baffle was compared. The results showed the effect of fluid structure interaction in the composite was significant and varied with the fluid fill level. In addition, the effect of a baffle varied between the sides of the structure with the most notable effect being on the front and back sides. The baffle provided the greatest strain reduction at the high fill levels.

14. SUBJECT TERMS glass fiber composite, fluid structure interaction, low velocity impact, partially filled fluid container			**15. NUMBER OF PAGES** 109
			16. PRICE CODE
17. SECURITY CLASSIFICATION OF REPORT Unclassified	**18. SECURITY CLASSIFICATION OF THIS PAGE** Unclassified	**19. SECURITY CLASSIFICATION OF ABSTRACT** Unclassified	**20. LIMITATION OF ABSTRACT** UU

THIS PAGE INTENTIONALLY LEFT BLANK

**FLUID-STRUCTURE INTERACTION IN A FLUID-FILLED COMPOSITE
STRUCTURE SUBJECTED TO LOW VELOCITY IMPACT**

Taylor J. South
Lieutenant, United States Navy
B.S., United States Naval Academy, 2006

Submitted in partial fulfillment of the
requirements for the degree of

MASTER OF SCIENCE IN MECHANICAL ENGINEERING

from the

**NAVAL POSTGRADUATE SCHOOL
June 2016**

Approved by: Young W. Kwon
                      Thesis Advisor

                      Jarema M. Didoszak
                      Second Reader

                      Garth V. Hobson
                      Chair, Department of Mechanical and Aerospace Engineering

THIS PAGE INTENTIONALLY LEFT BLANK

ABSTRACT

The effects of fluid structure interaction in a fluid-filled cubic composite structure subjected to low velocity impact are the focus of this study. A fabrication technique was developed for creating an E-glass composite cubic structure and a pendulum was designed and built to provide a repeatable low velocity impact. The behavior of the composite structure was studied at various fluid fill levels and impact velocities. The fluid level inside the structure was varied incrementally from empty (0% fill) to full (100% fill). With impact load measurements, strain measurements on each side, and high-speed video, the behavior for each test case was analyzed and compared. Two types of baffles were designed and fabricated out of dense foam material. The behavior of the structure with and without a baffle was compared. The results showed the effect of fluid structure interaction in the composite was significant and varied with the fluid fill level. In addition, the effect of a baffle varied between the sides of the structure with the most notable effect being on the front and back sides. The baffle provided the greatest strain reduction at the high fill levels.

THIS PAGE INTENTIONALLY LEFT BLANK

TABLE OF CONTENTS

LIST OF FIGURES

THIS PAGE INTENTIONALLY LEFT BLANK

LIST OF TABLES

THIS PAGE INTENTIONALLY LEFT BLANK

LIST OF ACRONYMS AND ABBREVIATIONS

CFRP	Carbon fiber reinforced polymer
fps	Frames per second
FSI	Fluid Structure Interaction
NI	National Instruments ®
NPS	Naval Postgraduate School
PMMA	Poly-Methyl Methacrylate
PVC	Poly-Vinyl Chloride

THIS PAGE INTENTIONALLY LEFT BLANK

ACKNOWLEDGMENTS

I would like to thank my advisor, Young Kwon, for introducing me to this interesting area of research and guiding me throughout my graduate education dedicated to this topic. His significant knowledge and experience in this field of research provided me with an incredible opportunity to advance my understating of the topics studied and structural mechanics in general. I would also like to thank Jarema Didoszak, John Mobley, and Chanman Park for their assistance throughout the experimental set-up and testing.

I would like to thank my parents for their reinforcement of education over the years and their continued support.

Most importantly, I would like to thank my lovely wife, Ashley, for her never-ending support and love, and uninterrupted encouragement. She has been patient through a cross-country move, understanding and tolerant during late nights and early mornings, my rock when times are tough, and my inspiration every day. Without her, I would not be the person that I am, and I would have been unable to achieve the milestones that I have.

Finally, I would like to acknowledge my late-night study buddy, Mr. Mont E. Monster. Thanks for hanging out with me while the rest of the world slept soundly in their beds.

THIS PAGE INTENTIONALLY LEFT BLANK

I.   INTRODUCTION

A.   BACKGROUND

Composite materials are becoming increasingly popular as they provide high stiffness and strength with low weight. They have a range of applications in the commercial and defense sectors, especially in the aerospace and marine environment. As these applications are usually in a dynamic setting, impact loading is a major area of interest. Composite structures are generally more vulnerable to impact damage than metallic structures due to their comparatively reduced hardness and ductility—the properties that allow metals to absorb greater amounts of energy without failure [1]. In addition, as composite structures are generally more flexible, greater deformation can occur following an impact. This can be a very important consideration when the composite structure is in close proximity to other structures or components. For instance, due to the limited space in an aircraft the fuel cell is often situated close to vital components. In the event of impact to the fuel cell, large deformations in the structure could cause unwanted contact with the adjacent components. Even if the composite structure does not fail, its dynamic response to the impact could cause damage to adjacent components. A representative fuel cell in a military helicopter is shown in Figure 1.

Composite structures containing a fluid, like a fuel cell, are subject to a dynamic interaction between the fluid and the structure, called fluid–structure interaction (FSI). This effect should be considered in composites as it differs considerably from metallic structures. The difference occurs because with a metal the density of the structure is much greater than that of the fluid, namely water. In a polymer composite, the densities of the structure and fluid are comparable, resulting in a very different structural response [2].

Figure 1.   Fuel Cell on MH-60 Blackhawk Helicopter. Source: [3].

B.   OBJECTIVE

The objective of this research is to understand the FSI effect on a composite structure filled with a fluid (water) and subjected to a low velocity impact. Understanding the dynamic response of the fluid filled structure can provide important information for future composite designs. It is important to understand the conditions that cause the greatest stress, strain, and deformation in the structure as well potential mitigating factors. Ultimately, the goal of the research is to provide insight into trends that can improve defense and commercial composite structures.

C.   EXPERIMENTAL OVERVIEW

An E-glass composite cubic structure was fabricated for testing and a pendulum was built to provide a repeatable low velocity impact. The effects of FSI were analyzed by incrementally varying the fluid fill level and measuring the impact force and strain

response on each side of the structure. Two baffles were designed and fabricated, and their effects on the structural response were evaluated.

The composite structure was fabricated by hand wrapping E-glass fabric around a cubic form that could be disassembled after curing. A predetermined number of wraps of the composite were used to achieve a wall thickness of approximately 2 mm. Biaxial strain gages were installed at the center of the side and back faces, and offset on the front (impact) face.

Impact tests were performed for various fluid fill levels including empty (0%), 25%, 50%, 75%, 90%, 95%, and full (100%). The impact was varied between a 25 degree drop angle and a 45 degree drop angle. The tests were repeated a minimum of six times to ensure consistency among the data. Adequate time was given between each impact to ensure that there was no residual fluid motion from the previous test.

D.   PRIOR RESEARCH

The majority of previous research completed on the topic of composite structural impact has not considered FSI. A numerical and experimental study conducted by Kim et al [4]. is an example of a case in which a composite structure was studied without the influence of FSI. In this study of impact force, deflection, and strain were measured in a carbon fiber reinforced polymer (CFRP) composite cylinder subjected to low velocity impact without the presence of a fluid. In some selected composite studies [5–7], FSI on a flat plate subjected to low velocity impact was analyzed. In two of these studies, the composite was a sandwich construction and in the third, the composite was E-glass and resin only. The research found that FSI had a significant effect on the dynamic response of a composite structure.

Research that has included structures containing a fluid have differed from the current study as the previous work has examined impacts via numerical analysis, slosh dynamics, impacts on metal structures, and high velocity impacts. In a study conducted by Firouz-Abadi et al. [8], only a numerical analysis was used to measure the modal frequencies and wall pressures in a flexible laminated composite at various liquid levels. Additional numerical studies that have been conducted were compiled and compared by

Rebouillat et al. [9]. While many of them included experimental validation, the common theme among the research of partially filled liquid containers was sloshing effects. Sloshing seems to be the dominant area of research related to composites structures filled with liquid. The experimental studies that have been conducted used a horizontal shaking excitation instead of a structural impact [10]. The effects of baffles have also been studied in these cases to determine their effect on sloshing, but not their effect in an impact [11].

When impacts on partially fluid filled containers have been studied it has either related to metal structures or high velocity impacts in composites. In a study conducted by Ince et al. [12], low velocity impacts were analyzed but the method and materials differed from the content of the research at hand. The box structures were constructed of steel and aluminum, and the impact force was applied by dropping the box structure from an elevated position vice striking it with a mass. Finally, research conducted by Artero-Guerrero et al. [13–14] and Varas et al. [15] was the most comparable in many ways. In these studies, fluid filled CFRP rectangular structures were measured for strain and pressure during a high velocity impact at various liquid levels. Because the impact was at high velocity, the focus of the research was on hydraulic ram effects on the fluid and structure.

There has been little research to date on fluid filled composite structures subjected to low velocity impact. The focus of this research is to provide more understanding in this area and provide recommendations for future composite design.

II. FABRICATION AND EXPERIMENTAL METHODS

A. COMPOSITE MATERIAL AND PROPERTIES

Composite structures can be constructed of many different materials, but many common marine and aerospace structures are made of E-glass woven fabrics and an epoxy. Within these materials lie various types that can be selected based on the specific application. Each of the various material types have different properties associated with them. The discussion below provides specific details for the properties of the materials used to fabricate the composite structure for this experiment.

1. E-Glass

The E-glass woven fabric used to fabricate the composite structure was a 6 ounce bi-directional woven fabric as shown in Figure 2. This woven fabric is common with in the fiberglass industry and can be purchased in a rolled form from various vendors.
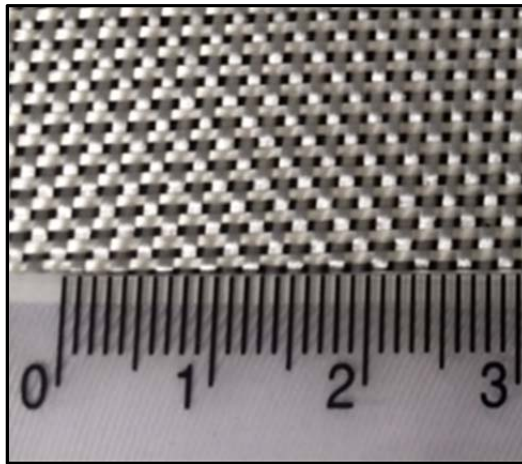
Figure 2.   E-Glass Bi-directional Woven Fabric.

2. Resin and Hardener

The resin and hardener used to fabricate the composite structure was a toughened laminating epoxy manufactured by Pro-Set®. The specific resin and hardener combination used was the M1002 resin and M2046 hardener (Figure 3). The hardener

was chosen to allow for a working time suitable for the fabrication process for the structure. For this epoxy, the working time could be between 4.5 to 6 hours, depending on the amount of hardener used in the mixture. The specific technical data for the epoxy is shown in Figure 4 [16].

Figure 3.   Pro-Set® Resin and Hardener.

HANDLING PROPERTIES

Property	Standard	Units	72°F (22°C)
100g Pot Life	ASTM D2471	minutes	72-88
Viscosity Mixed	ASTM D2196	cP	2,100
Viscosity (resin)	ASTM D2196	cP	4,800
Viscosity (hardener)	ASTM D2196	cP	115

MIX RATIO

Method	Resin:Hardener	Range	Resin:Hardener	Range
Weight	4.17:1	3.83:1–4.78:1	100:24.0	100:26.10–100:20.90
Volume	3.57:1	3.16:1–3.95:1	100:28.0	100:31.60–100:25.30

DENSITY

State	Units	72°F (22°C)
Cured	lb/gal (g/cc)	9.81 (1.17)

MECHANICAL PROPERTIES

Property	Standard	Units	RT Gelation + 140°F (60°C) x 8 hrs	RT Gelation + 180°F (82°C) x 8 hrs
Hardness	ASTM D2240	Type D	83	83
Compression Yield	ASTM D695	psi (MPa)	14,100 (97)	13,900 (96)
Tensile Strength	ASTM D638	psi (MPa)	10,000 (69)	9,590 (66)
Tensile Modulus	ASTM D638	psi (MPa)	4.33E+05 (2.99)	3.94E+05 (2.72)
Tensile Elongation	ASTM D638	%	5.5	5.7
Flexural Strength	ASTM D790	psi (MPa)	18,800 (130)	1,770 (12)
Flexural Modulus	ASTM D790	psi (MPa)	5.55E+05 (3.83)	5.14E+05 (3.54)

Figure 4.   Pro-Set® Material Data and Properties.

3.   E-Glass / Epoxy Composite

The E-glass and epoxy combination similar to the one used in this experiment was studied extensively by Miller [17]. In his research Pro-Set ® M237 hardener was used vice the M2046 hardener used in this experiment. The difference between the two hardeners is the cure time. The results of Miller's study are shown in Figures 5 and 6. The room temperature properties are the assumed material properties for the composite structure used in this experiment.

Ultimate Strength of Composite (Pa)			
Room Temperatures		Cold Temperatures	
1–1	2.65E+08	1–2	2.47E+08
1–3	2.65E+08	1–4	2.36E+08
2–3	2.42E+08	1–5	2.76E+08
2–4	2.37E+08	2–2	2.20E+08
2–5	2.23E+08		
Average	2.46E+08	Average	2.45E+08
Standard Deviation	1.63E+07	Standard Deviation	2.05E+07
Difference (Pa)	-0.01E+08	Difference (%)	-0.4%

Figure 5.   Composite Ultimate Tensile Strength.

Young's Modulus of Composite (Pa)			
Room Temperatures		Cold Temperatures	
1–1	1.02E+10	1–2	9.73E+09
1–3	1.06E+10	1–4	9.40E+09
2–3	1.00E+10	1–5	9.96E+09
2–4	1.00E+10	2–2	9.08E+09
2–5	9.95E+09	2–1*	9.06E+09
Average	1.02E+10	Average	9.44E+09
Standard Deviation	2.37E+08	Standard Deviation	3.12E+08
Difference (Pa)	7.60E+08	Difference (%)	7.45

Figure 6.   Composite Young's Modulus.

B.   COMPOSITE STRUCTURE GEOMETRY

For this experiment, a cubic geometry was selected as the structure of interest. This structural shape could be applied to many practical applications, related to previous research, and more easily modeled using numerical modelling software. The interior dimensions of the cube were chosen to be 25 cm x 25 cm x 25 cm. The walls of the cube were to be made of composite with an open top and bottom. A base plate would support one side of the structure and the other side covered with a top plate. The desired thickness of the composite structure was approximately 2 mm. For referencing the composite structure throughout the experiment, the axes and sides were provided labels as shown in Figure 7.
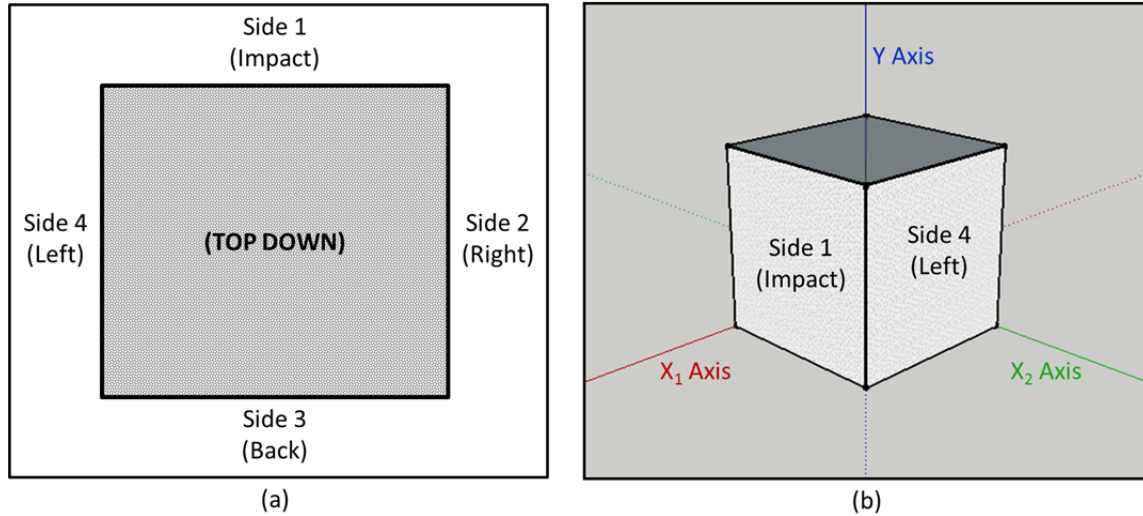
Figure 7.   Side Label and Axis Reference From (a) Top-Down View and
(b) Isometric View.

C.   COMPOSITE STRUCTURE FABRICATION

In preparation for fabricating the cubic composite structure, past composite research projects by Violette [5], Conner [6], and McCrillis [7] were reviewed. Additionally, engineering journal articles [15, 18] were studied, and online composite structure resources were consulted [19]. It was determined that a common composite fabrication method for three-dimensional structures involved building the E-glass and resin around a form. With the E-glass and resin built around the form the entire structure would cure while under vacuum as was a common composite fabrication method in past NPS research projects.

1.   Composite Form

The composite form was designed such that it could be disassembled and removed from the inside of the structure after fabrication. In order to accomplish this, the form design consisted of acrylic plates clamped between aluminum angle fastened together by nuts and bolts. The raw materials for the form were 91.44 cm x 30.48 cm x 0.635 cm acrylic plate, 5.08 cm x 5.08 cm x 0.635 cm aluminum angle, and 2.54 cm x 2.54 cm x 0.635 cm aluminum angle. The acrylic plate was cut in to 12 pieces; four plates that were 32 cm x 14.8 cm to make the sides, and eight pieces that were 26 cm x 7.5 cm

to be connecting tabs. With the acrylic cut to shape, the eight smaller pieces were adhered to the four larger plates using PVC pipe cement. These tabs allowed the form sides to be securely clamped between the aluminum angle. One of the completed form sides is shown in Figure 8. The aluminum angle was cut into 60.96 cm length pieces and 0.635 cm holes drilled to facilitate bolting the angle together. The cut and drilled aluminum angle ready for assembly is shown in Figure 9.
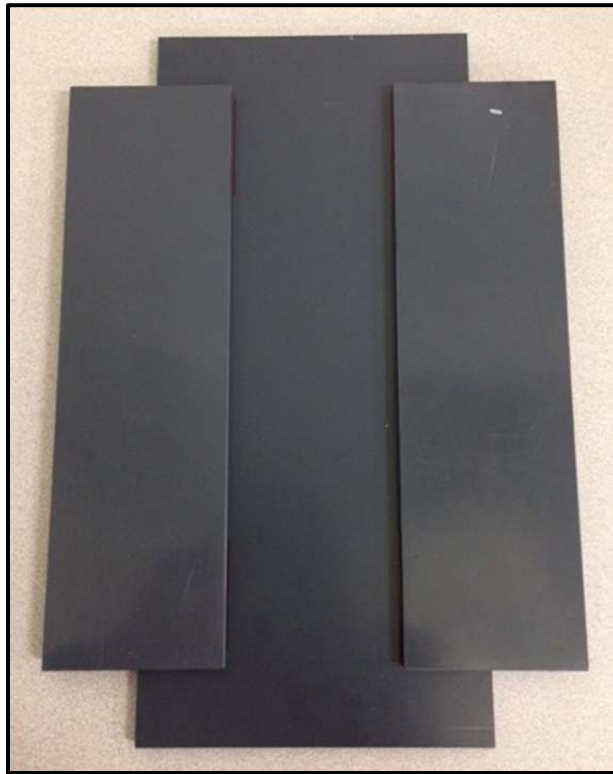
Figure 8.   Assembled Side of Composite Form.
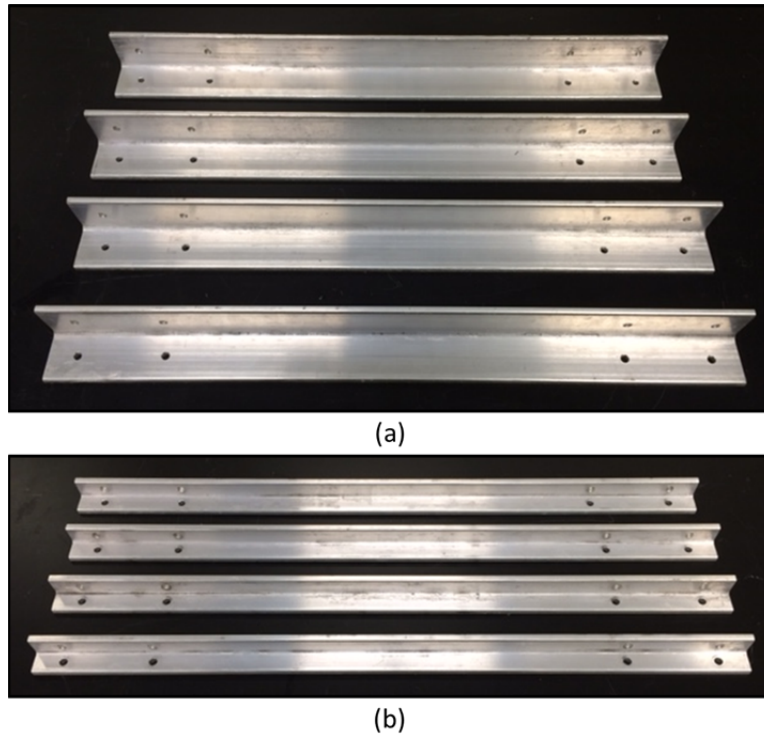
Figure 9.   (a) 5.08 cm Angle and (b) 2.54 cm Angle Cut and Drilled
for the Composite Form.

2.   Fabrication Procedure

With the form pieces built to the designed specifications, the fabrication process was completed by assembling the form, cutting the E-glass fabric to fit the form, measuring and mixing the resin and hardener, building the E-glass and epoxy around the form, placing the completed composite under vacuum, allowing it to cure completely, and disassembling and removing the form.

a.   Form Preparation

The acrylic sides of the form were placed between the aluminum angle and the bolts tightened to hold the sides securely in place. The assembled form is shown in Figures 10 and 11. In order to prevent the epoxy from adhering to the acrylic or aluminum, a layer of wax paper was taped to the exterior of the form. The form was supported between two chairs to allow access to all sides during the composite layup and allowed it to be easily rotated throughout the layup process.

11

Figure 10.   Assembled Composite Form (side).
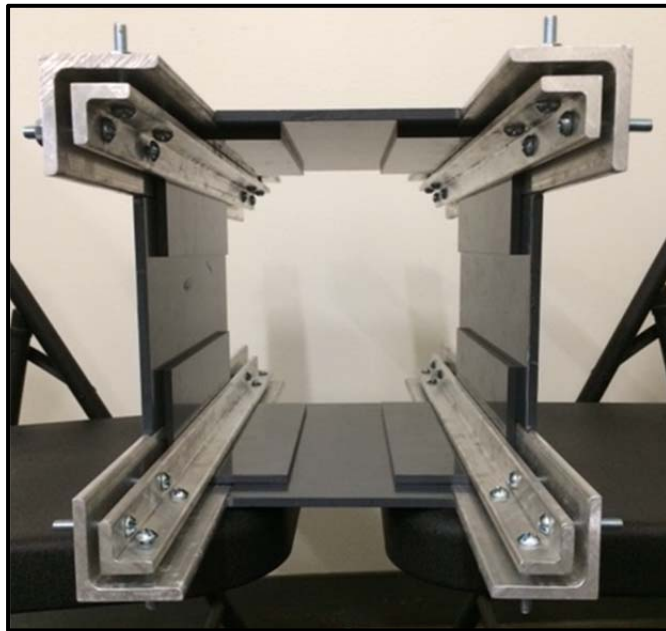
Figure 11.   Assembled Composite Form (end).

b.   *E-Glass / Epoxy Preparation*

In preparation for the composite layup, several flat samples were made to determine the proper number of E-glass layers needed to acquire the desired composite

thickness of 2 mm. Based on the samples it was determined that eight layers of E-glass and epoxy would achieve the desired thickness.

In creating the composite structure, the E-glass fabric was to be wrapped around the form in as continuous a process as possible, as to minimize seams and discontinuities in the E-glass. Through the fabrication of several practice composite structures using the form, it was determined that a maximum of four wraps (layers) could be made around the form with one continuous piece of E-glass fabric. With longer fabric pieces, it was very difficult to manage the amount of excess fabric during the first two wraps (layers). With this information it was determined that the best fabrication process would include three E-glass fabric sheets of 275 cm each. This length allowed a seam to fall on each corner for consistency, and made one of the sides a layer thicker than the others. The side with the extra (9th) layer was the impact face and allowed for increased strength through repeated impacts during testing. The wrap (layer) pattern used for fabricating the composite structure is shown in Figure 12. Each E-glass fabric sheet measured 275 cm x 28 cm, as shown in Figure 13. The excess width allowed the top and bottom edges to be trimmed to a straight edge after curing.
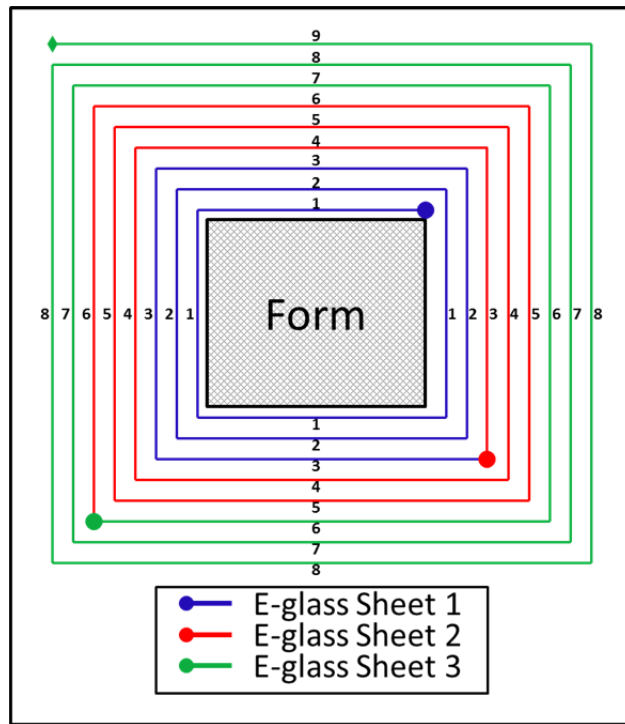
Figure 12.   E-Glass Wrap (layer) Pattern around the Form.

Figure 13.   Roll of E-Glass Ready to be Cut into Layers
for Composite Fabrication.

The epoxy was prepared using Pro-Set® M1002 resin and M2046 hardener. The ratio of resin to hardener was determined using the weight method, and a value chosen between the allowed ranges of 3.83:1 to 4.78:1. The amounts of resin and hardener used were 499.9 g and 117.8 g, respectively, and were mixed thoroughly.

c.   *Composite Layup*

The form was positioned as to allow it to be rotated throughout the layup process, making the top surface the working surface. A layer of epoxy was laid to cover the wax paper and provide a surface to which the E-glass fabric could adhere. This process was repeated on each side of the form as the first layer of the E-glass was laid. Special attention was given to ensure that the first layer of E-glass and epoxy was tightly fitted around the form and especially at the corners. The first layer of E-glass fabric laid on the form is shown in Figure 14.
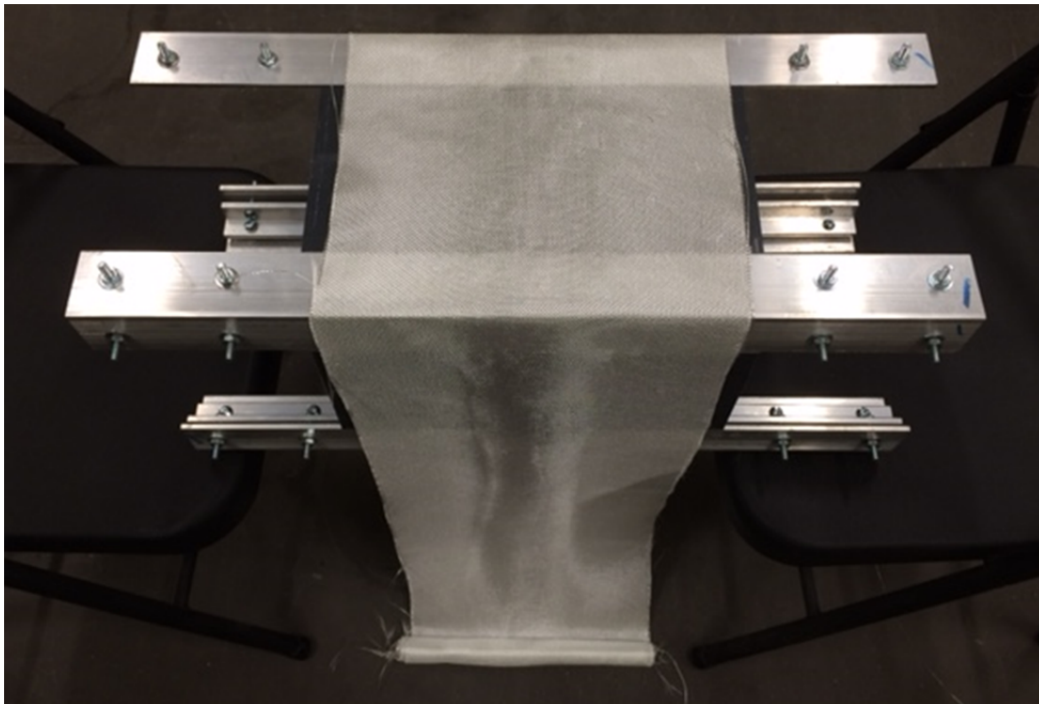
Figure 14.   First layer of E-Glass Laid on Form During Fabrication.

The wrapping of the E-glass layers was continued, rotating the form as each side was covered with a new layer of E-glass and thoroughly wetted with epoxy. The epoxy

was poured onto the top surface (working side) and spread across the entire surface using a plastic applicator (squeegee). After the entire surface was fully wetted, any excess epoxy was moved to the next working side as the form was rotated. When the second and third E-glass fabric sheets were added, the sheets were carefully placed so that they butt against the end of the previous sheet.

When the final layer of the E-glass fabric was laid on the form and wetted with epoxy, the composite was covered with a layer of perforated plastic. An absorbent cloth was then placed over the perforated plastic in order to removed excess epoxy when the composite was placed under vacuum. The layers of materials used in the composite layup are shown in Figure 15.
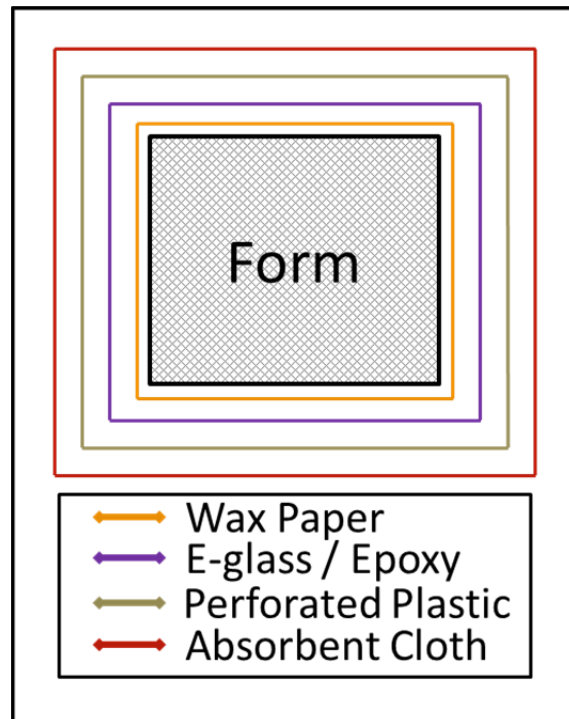
Figure 15.   Material Layers for Composite Fabrication.

d.   *Vacuum Set-up*

After completing the fabrication of the composite structure, and with all layers of materials added (Figure 15), the form was prepared to be placed under vacuum. To prevent puncture of the vacuum bag, the sharp corners of the aluminum angle and bolt

16

ends were covered with double-sided gasket tape. The form was then placed inside a large heavy weight trash bag, with an additional inflated bag placed in the center of the form. The inflated bag prevented the vacuum bag from collapsing into the center of the form and tearing. The vacuum hose was inserted and made air tight with double-sided gasket tape. Finally, the composite structure was placed under 68.95 kPa of vacuum and held for 1.5 hours. The composite structure under vacuum is shown in Figure 16.

Figure 16.   Form and Composite Under Vacuum After Layup.

e.   *Composite Curing*

The composite structure was allowed to cure for 24 hours after fabrication. When completely cured, the vacuum bag, absorbent cloth, and perforated plastic were removed and discarded. The bolts were then removed from the form so that the 2.54 cm interior aluminum angle could be removed, followed by the acrylic side plates, and finally the

5.08 cm exterior aluminum angle. The wax paper that had been the boundary between the form and composite structure was then peeled from the inside of the structure.

3. Post Fabrication Preparation

The composite structure required additional work after fabrication in order to make it ready for experimental testing. The top and bottom edges of the structure were cut to provide the proper testing dimensions, and uneven areas were sanded or filled to provide a smooth and consistent surface. Then, the impact point was reinforced to support repeated impact tests, strain gages were installed for data collection, and the exterior surfaces were painted.

a. Sizing

The top and bottom edges of the composite structure were rough due to the edges of the E-glass fabric not perfectly aligning in each layer of the fabrication process. To remove this excess composite and size the structure to the dimensions needed for testing, the top and bottom were cut to a straight edge. The overall height of the box was to be 28 cm (as 1.5 cm were fixed in the base plate and 1.5 cm were fixed in the top plate). To cut the straight edges, 14 cm were measured from the center to the top and bottom of composite structure. The top and bottom edges were made square to the sides, and cut with a Dremel ® Rotary Tool fitted with a diamond cutting wheel. The composite structure after being cut to size is shown in Figure 17.
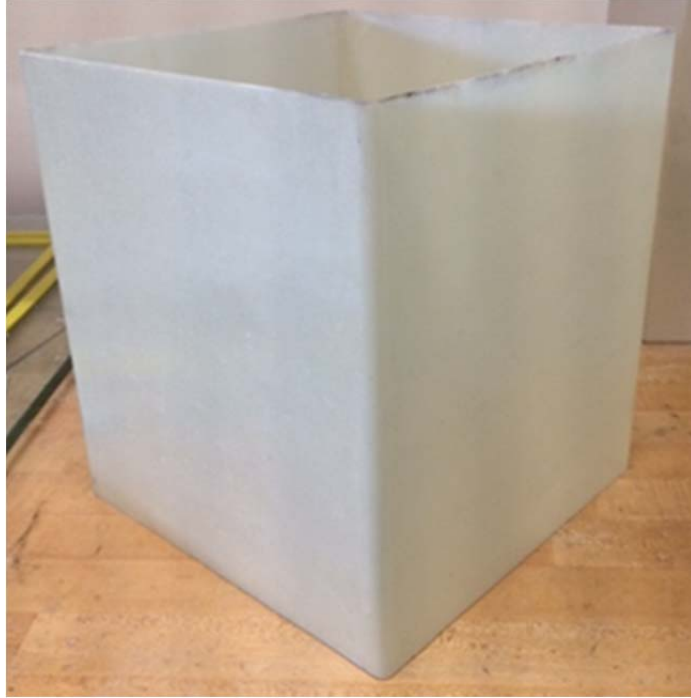
Figure 17.   Composite Structure Cut to Size for Testing.

b.   *Surface Finish*

To prepare the interior and exterior surfaces of the composite structure for testing, minor finishing was needed. Several areas required epoxy filling and several areas required light sanding. The epoxy filling was required on the inside corners of the structure. Through the fabrication and curing process several voids were developed, two of which can be seen in Figure 18.
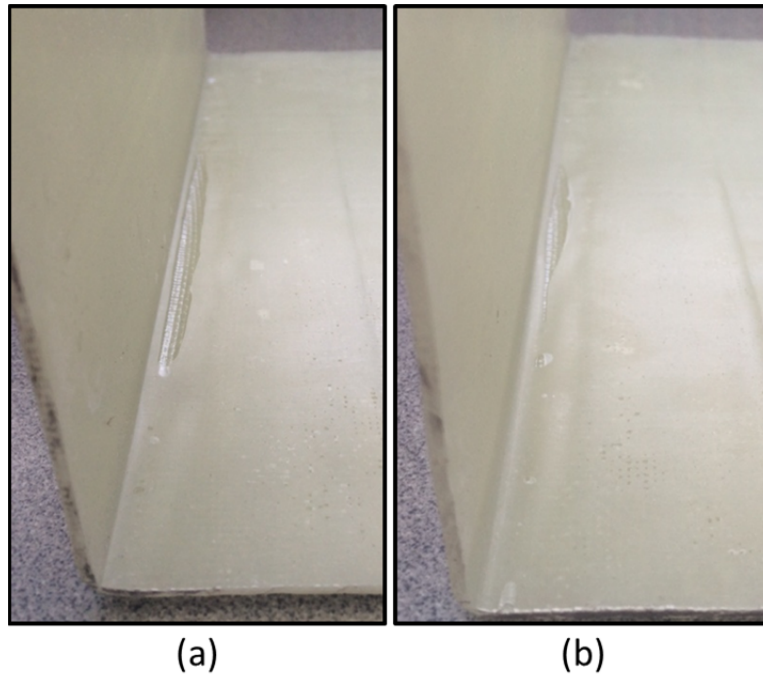
Figure 18.   Examples of Resin Voids in the Interior Corners at the
(a) Front-Right Side and (b) Back-Left Side.

Because the voids were located on multiple faces, they were filled one at a time and allowed to completely cure before moving to the next face. The epoxy ratios for each void fill are listed in Table 1.

Table 1.   Ratio of Epoxy Used to Fill the Voids

Void Fill	Resin	Hardener
Void Fill 1	60.0 g	15.5 g
Void Fill 2	11.6 g	3.9 g
Void Fill 3	12.0 g	3.2 g
Void Fill 4	13.9 g	3.6 g

On the exterior surface of the composite structure, the absorbent cloth did not remove several high areas of epoxy during the vacuum process. These areas were lightly sanded with 500 grit sand paper making sure to not damage the E-glass fibers.

When the surface finish was in a condition that it was ready for testing, the thickness of the composite structure was measured and recorded. A digital caliper was

used to measure the thickness at three locations on the top and bottom of each side. The locations measured are shown in Figure 19 and their respective thicknesses are listed in Table 2. The bottom thicknesses are larger than the top thicknesses due to the gravity forces on the epoxy during the curing process. Additionally, the thicknesses on side 4 (left) are slightly greater than the other sides. This is attributed to the amount of excess epoxy that was absorbed during the vacuum bag process and curing being slightly less than that of the other sides. The average thickness for all sides was 2.114 mm.
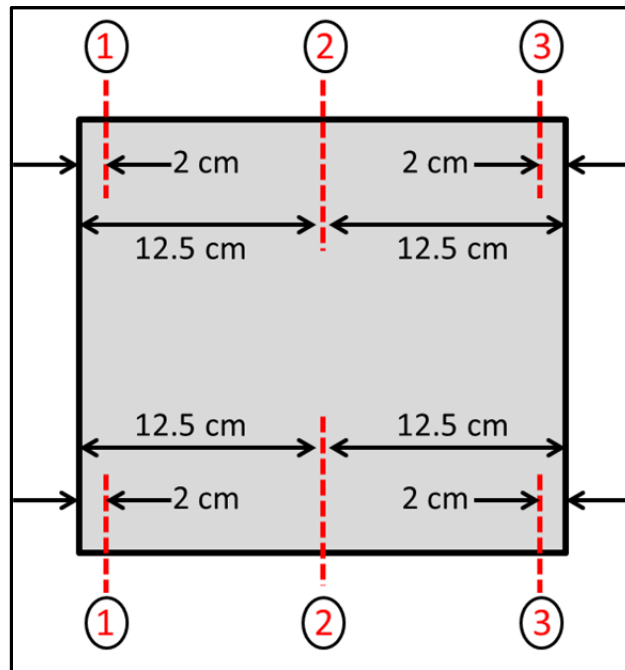
Figure 19.   Thickness Measurement Locations.

Table 2.   Composite Thickness Measurements.

Location	Thickness	Location	Thickness
Side 1 (Impact)			
Top 1	1.76 mm	Bottom 1	2.14 mm
Top 2	1.92 mm	Bottom 2	2.32 mm
Top 3	1.99 mm	Bottom 3	2.32 mm
Side 2 (Right)			
Top 1	1.90 mm	Bottom 1	2.15 mm
Top 2	1.96 mm	Bottom 2	2.37 mm
Top 3	1.56 mm	Bottom 3	1.78 mm
Side 3 (Back)			
Top 1	1.94 mm	Bottom 1	2.16 mm
Top 2	2.06 mm	Bottom 2	2.54 mm
Top 3	1.89 mm	Bottom 3	2.29 mm
Side 4 (Left)			
Top 1	2.22 mm	Bottom 1	2.34 mm
Top 2	2.37 mm	Bottom 2	2.36 mm
Top 3	2.12 mm	Bottom 3	2.27 mm

c.   *Impact Point Reinforcement*

Because the front face of the composite structure would experience repeated impacts during testing, the impact point was reinforced in order to prevent damage to the composite. A 3.81 cm x 3.81 cm x 0.3175 cm piece of 6061 aluminum plate was adhered to the center of the front face. The aluminum square was adhered with the same epoxy used throughout fabrication and surface finish process. The aluminum square installed at the impact point is shown in Figure 20.
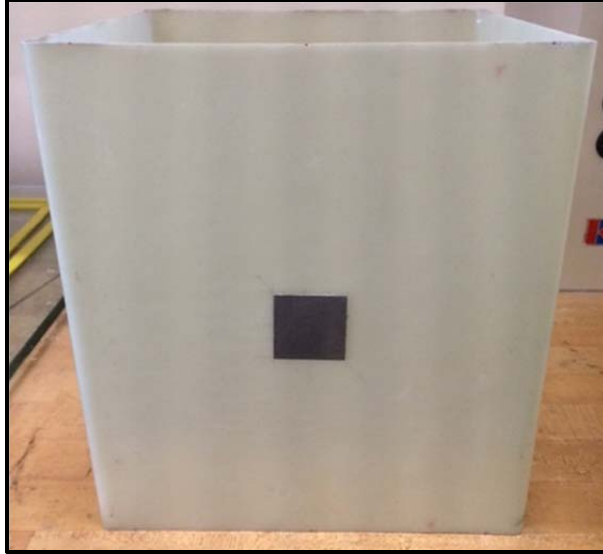
Figure 20.   Aluminum Impact Point Reinforcement.

d.   *Strain Gage Installation*

Strain gages were used to measure the strain in the x-direction and y-direction on each face of the composite structure. The strain gages were located at the center of the side faces and back face. Because the front face was impacted at the center, the strain gage on that face was offset. Figure 21 depicts where the strain gages were installed.
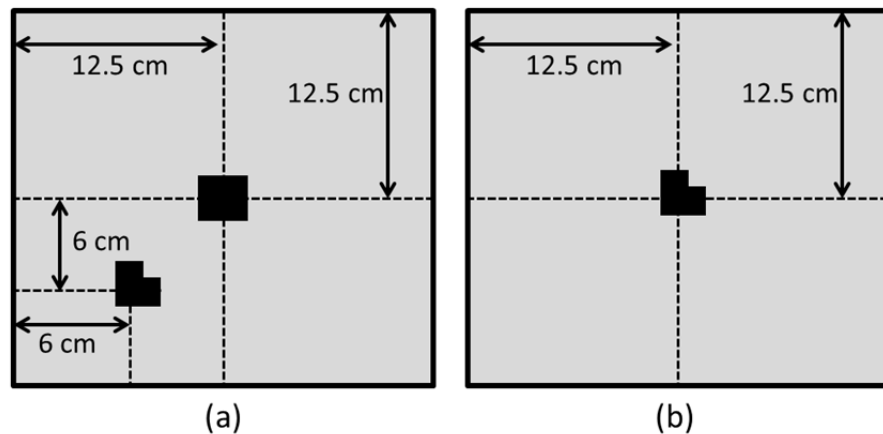
Figure 21.   Strain Gage Locations on (a) the Front Side and
(b) the Left, Right, and Back.

23

The biaxial (0° / 90°) rosette strain gages were manufactured by Micro-Measurements® (Part Number CEA-13–125WT-350). The gages had a grid resistance of 350 ohms and nominal gage factor of 2.15.

To install the strain gages on the composite structure the following procedure was used. The procedure was adapted from previous composite research [20].

Application of Strain Gages—the following procedure was used to apply strain gages to all sides of the composite structure:

1. Prepare Surface: The location for each strain gage was smoothed with a fine grit sand paper to remove imperfections. Following sanding, the surface was cleaned using a gauze pad soaked with ethanol followed by another gauze pad soaked with methanol.

2. Place Strain Gage: A small piece of cellophane tape was applied to the strain gage location and the used to hold the strain gage in place during curing.

3. Apply Bonding Agent: A Micro-Measurements M-Bond AE-10 Adhesive kit containing a two-part epoxy, dropper, and stir stick was used to bond the strain gages to the cylinder. The dropper was used to measure the appropriate amount of hardener for mixing with the resin for the designated five minutes. Following mixing, the stir stick was used to apply a small amount of epoxy to the strain gage. The strain gage and tape were then firmly pressed onto the side of the composite structure.

4. Wire leads: Following a 24 hour cure, the tape was removed and a dental tool was used to remove an excess resin from the solder pads on the strain gage. The lead wires were then soldered to the pads on the strain gages.

e.   *Painting and Speckle Pattern*

The exterior of the composite structure was prepared with a speckle pattern so that it could be analyzed for full field displacement and strain using digital image correlation. The speckle pattern was created using white and black spray paint as well as a bristle brush. The strain gages and impact reinforcement were covered with painters tape and entire exterior surface was painted white. The surface was allowed to dry thoroughly before the black speckle pattern was applied. To create the pattern, a bristle brush was coated with black spray paint and then the brush agitated to cover a small area

of the surface. This process was repeated until the speckle pattern was applied to an entire side. The structure was rotated and the pattern repeated. A representative section of the speckle pattern is shown in Figure 22.

Due to equipment limitations, the digital image correlation technique could not be used in this experiment. Because the limitations were not known during the fabrication phase, the structure was prepared with the speckle pattern to support the use of this technique in future research.

Figure 22.   Speckle Pattern for Digital Image Correlation.

4.   Baffle Fabrication

One of the areas to be analyzed in this study was the effect of a baffle on the fluid wave propagation within the composite structure. Two baffles were designed and fabricated using Divinycell vinyl foam. The foam was 7.5 mm thick and had a density of 0.045 g/cm3. The pores of the foam were small allowing a minimal amount of water to absorb into the foam when placed in the composite structure for testing. A close up picture of foams material structure is shown in Figure 23.
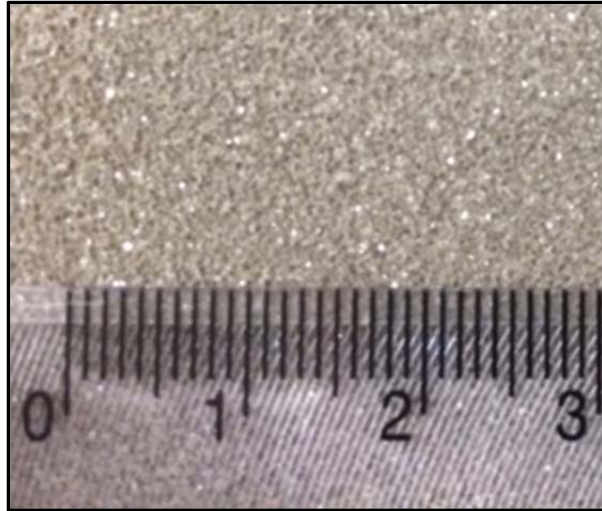
Figure 23.   Close Cell Vinyl Foam for Baffles.

a.   Baffle 1

The first baffle (Baffle 1) was a simple design resembling a "X" shape. Each panel measured 24 cm x 24 cm, and contained six 3 cm x 3 cm holes to allow fluid flow. The design of Baffle 1is shown in Figure 24.
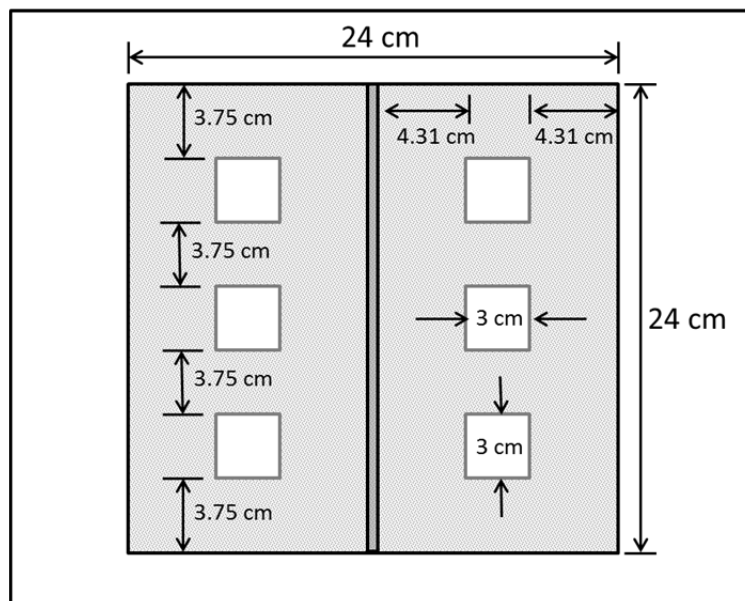
Figure 24.   Baffle 1 Design.

The foam was cut to the designed dimensions for the baffle and assembled. The two slots in the center of each panel were fitted together and small brad nails inserted at the top and bottom unions to secure the panels. The nail locations are depicted in Figure 25 (internal nail location noted in red) and the completed baffle shown in Figures 26 and 27.
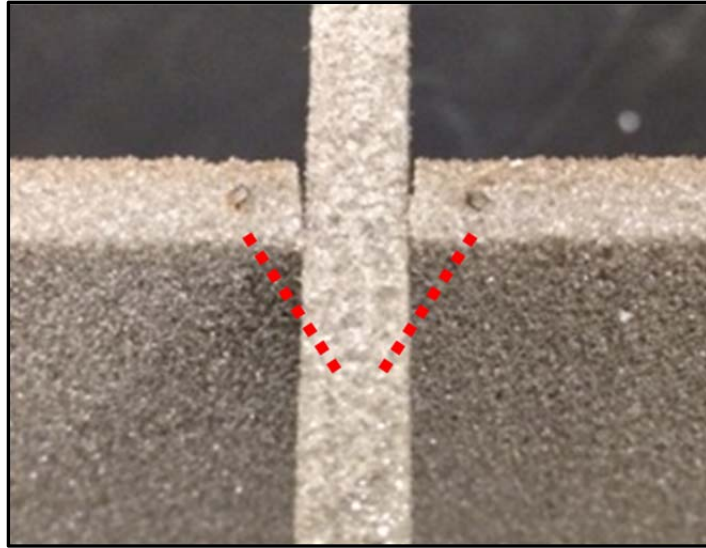
Figure 25.   Brad Nail Locations a Baffle Wall Connection.
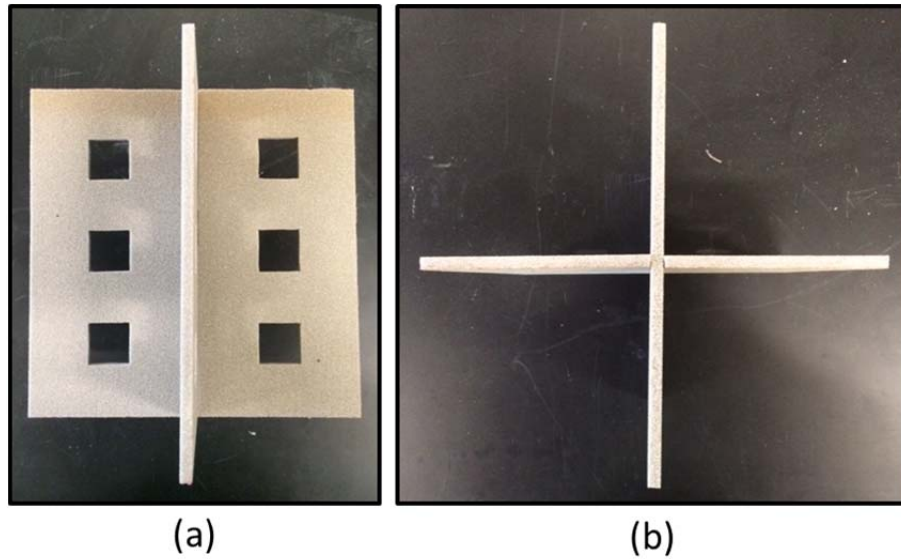
Figure 26.   Baffle 1 (a) Side Profile (b) Top Profile.
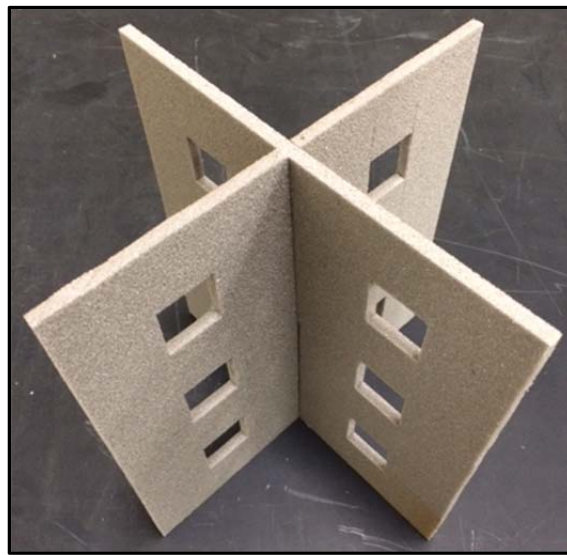
Figure 27.   Baffle 1 Isometric View.

b.   Baffle 2

The second baffle (Baffle 2) was a more complex design resembling a checker board shape. Each panel measured 24 cm x 24 cm, and contained nine 2 cm x 3 cm holes to allow fluid flow. Although the sizes of the holes differed from those used in Baffle 1, the total area of the holes in each panel was the same. The design of Baffle 2 is shown in Figure 28.
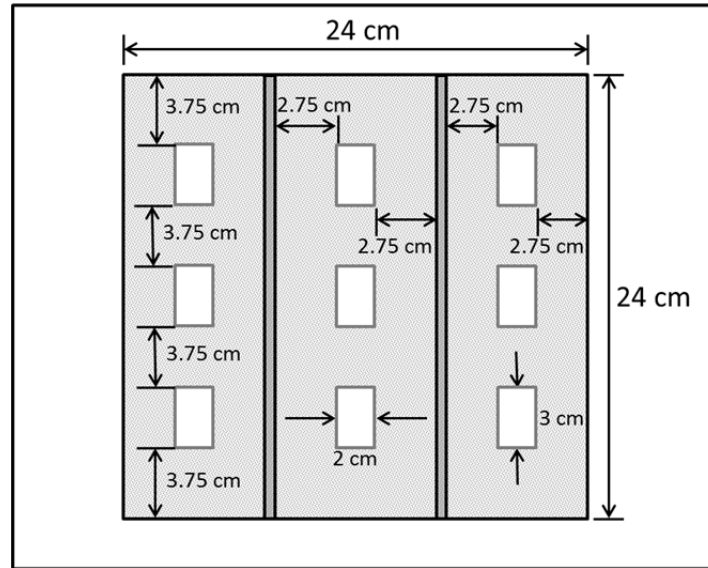
Figure 28.   Baffle 2 Design.

The foam for this baffle was cut and assembled in the same way as Baffle 1. The slots in each panel were fitted together and each union on the top and bottom secured with small brad nails (same as Baffle 1). The completed baffle is shown in Figures 29 and 30.
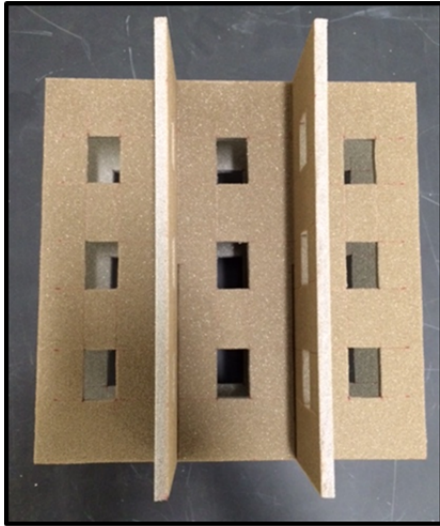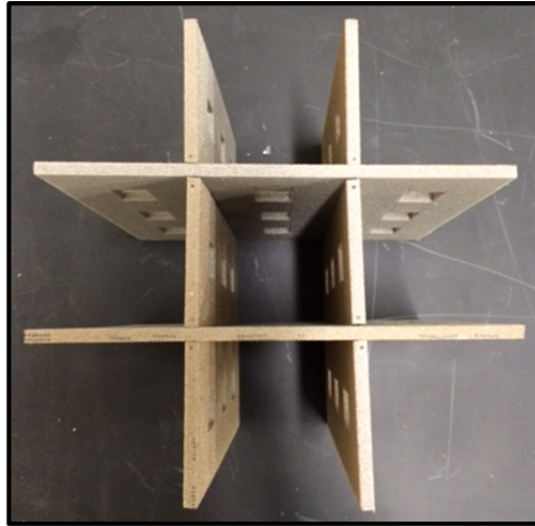
Figure 29.   Baffle 2 (a) Side Profile (b) Top Profile.
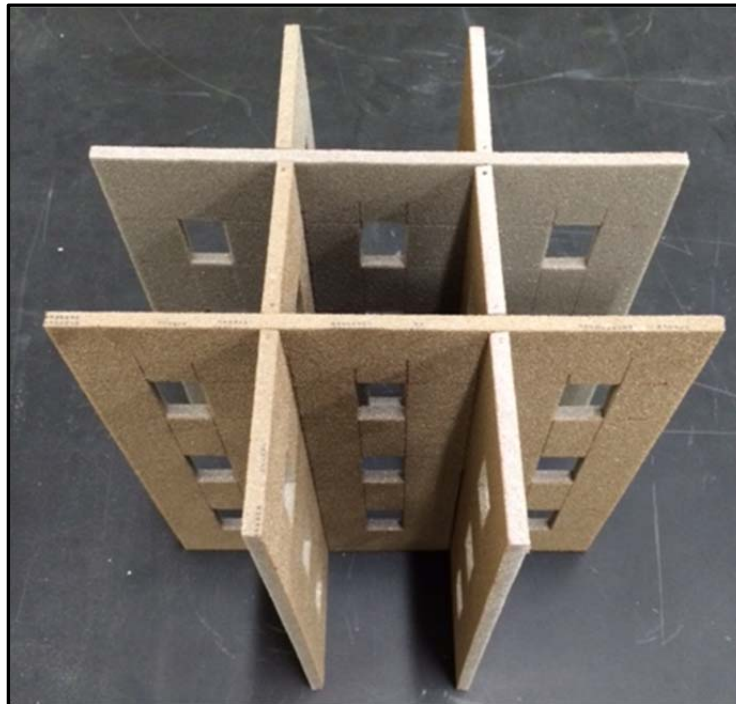
Figure 30.   Baffle 2 Isometric View.

D.   TEST EQUIPMENT AND SET-UP

The test set-up included an impact pendulum, the composite structure fixed to a base plate and top plate, strain gages and a load cell connected to a data acquisition computer, and a high-speed camera.

1.   Impact Pendulum

The impact pendulum consisted of four major components: a support stand, a mounting plate and rotating rod, a pendulum arm, and a hemispherical impactor with an inline load cell.

a.   *Pendulum Support Stand*

The impact pendulum was supported by a Lateral Excitation Stand (Model 2050A) produced by The Modal Shop Incorporated [21]. The pendulum was attached to the collar on the lateral arm and could be adjusted along the length of the arm. The lateral arm was also able to be adjusted along the y-axis to ensure that the impactor was precisely aligned to the center of the composite structure. The stand was adjusted and aligned such that that the tip of the impactor was in contact with the aluminum impact plate when at rest. Because the stand was able to rotate about the y-axis, it was bolted to the test table as shown in Figure 31. The table used for the experiment was a Sealed Hole Table Top with Tuned Damping (RS 4000) supported by Stabilizer High Performance Laminar Flow Isolators (S-2000 Series) produced by Newport Corporation [22–23]. The stabilized isolators were not activated during testing.
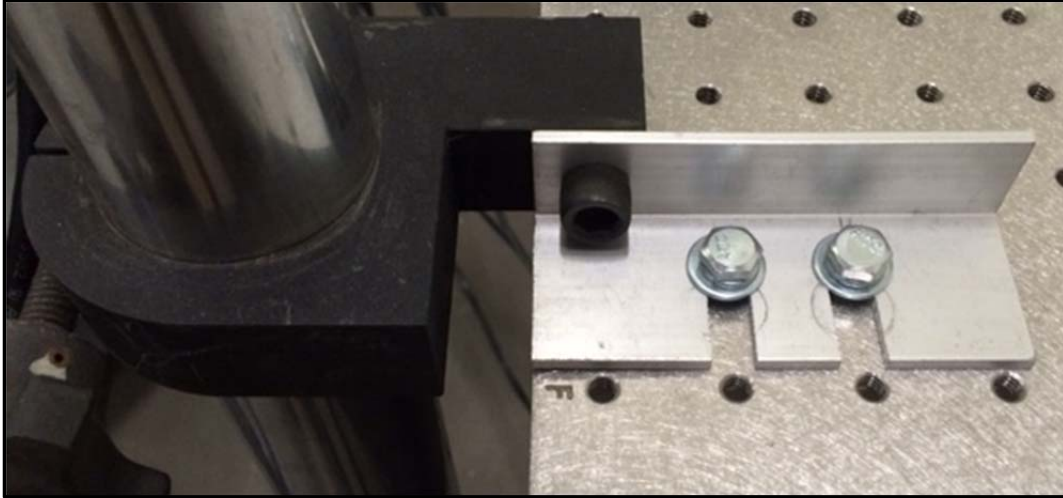
Figure 31.   Impact Pendulum Secured to Table Top.

b.   *Mounting Plate and Rotating Rod*

A mounting plate was fabricated from 6061 aluminum plate that was 30.48 cm x 20.32 cm, and 0.635 cm thick. Holes were drilled through the plate as shown in Figure 32, and the plate mounted to the test stand collar using 3/8–16 U-bolts. A 6061 aluminum tube that was 30.48 cm long, with outer diameter of 2.54 cm and wall thickness of 0.635 cm, was secured in two pillow block mounted roller bearings. The roller bearings were bolted to the base plate providing the axis of rotation for the pendulum as shown in Figure 33.
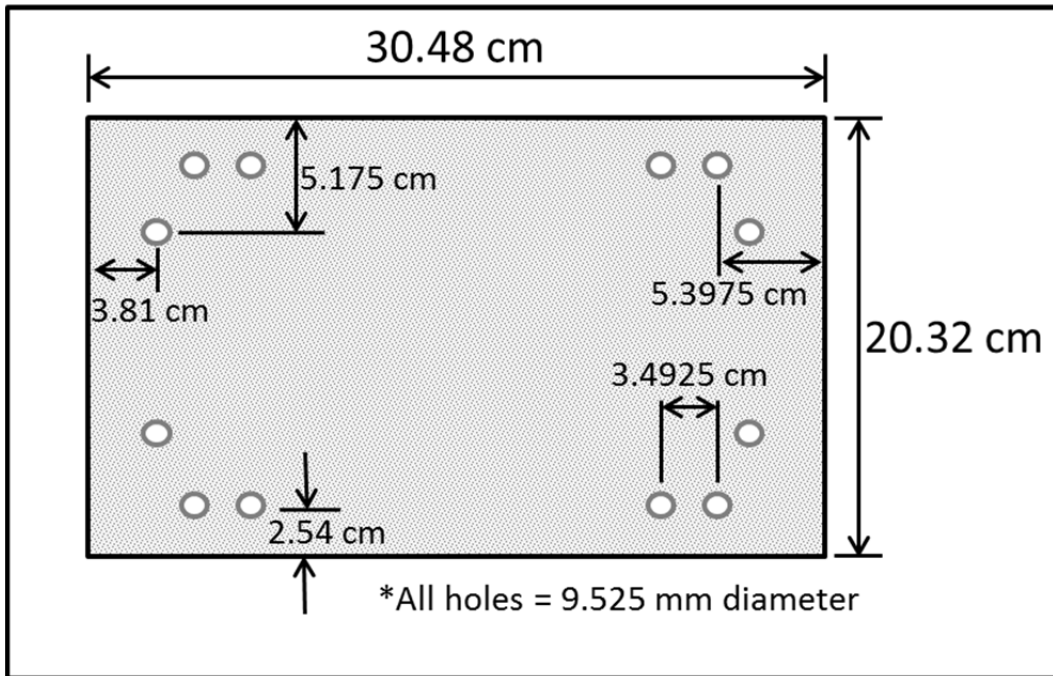
Figure 32.   Mounting Plate Design.
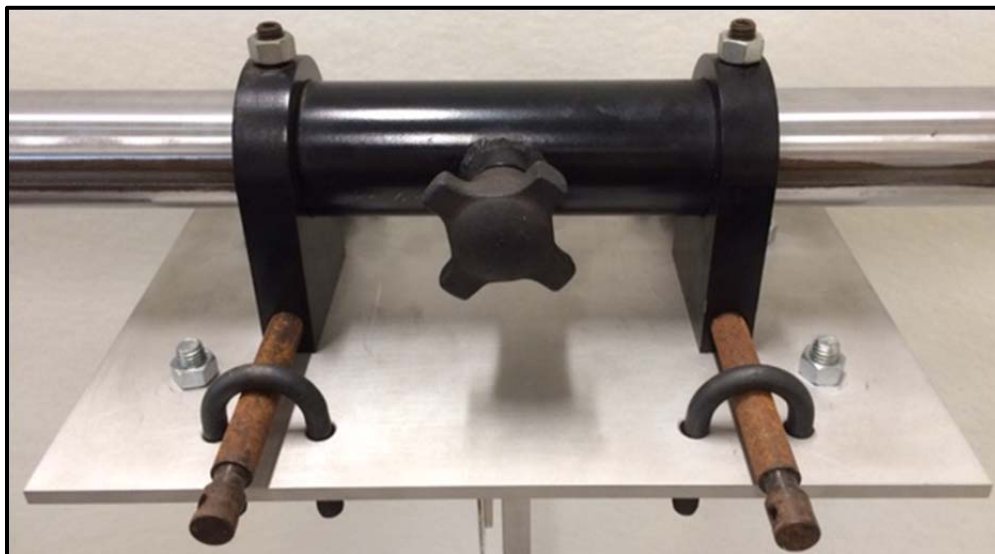
Figure 33.   Mounting Plate on Pendulum Support Stand.

To measure the angle of the pendulum a protractor was fixed to the bottom of the mounting plate with the 0-degree mark aligned to the center of the axis of rotation and pendulum arm, as shown in Figure 34.
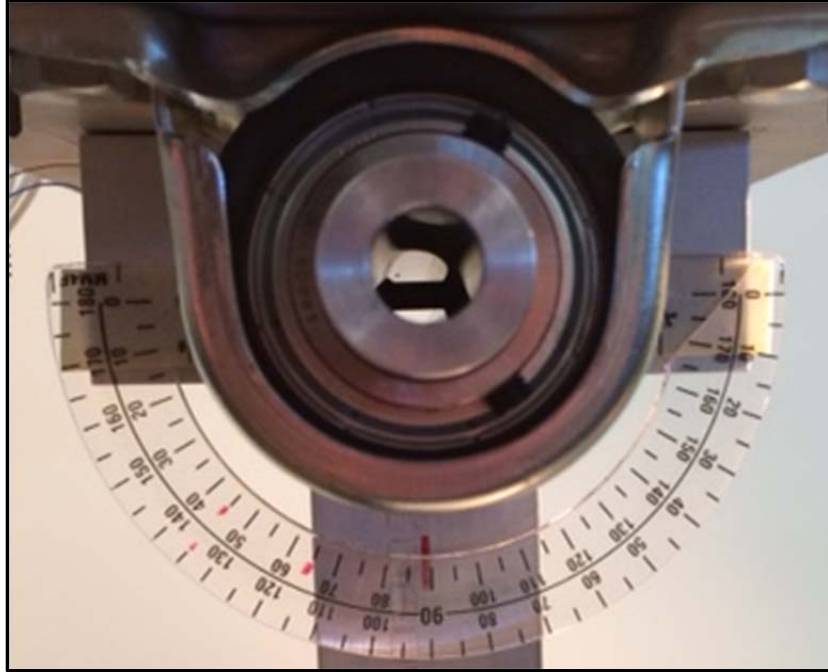
Figure 34.   Protractor and Pendulum Arm for Drop Angle Measurement.

c.   *Pendulum Arm*

The pendulum arm was fabricated from 6061 aluminum flat bar that measured 57.15 cm x 5.08 cm x 1.27 cm. At the top of the flat bar (arm) a 2.54 cm diameter hole was drilled to accommodate the aluminum tube (shaft). A 2.54 cm diameter hole was also drilled through the arm and shaft and fitted with a 0.9525 cm bolt and nut to bond the two pieces (Figure 35). A 2.54 cm radius was cut on the top of the arm to prevent contact with the mounting plate through the range of pendulum rotation.

Figure 35.   Attachment Point for Rotating Rod and Pendulum Arm.

At the bottom of the arm two holes were drilled on the back side to accommodate a brass bar for added mass. The brass bar, shown in Figure 36, measured 15.56 cm x 2.54 cm x 1.27 cm, and weighed 434.5 g. An additional hole was drilled on the front of the arm as a threaded connection point for the impactor. This hole was located 1.27 cm from the bottom of the arm; drilled to a depth of 1.27 cm and tapped for a 1/4–28 thread. The completely assembled pendulum arm is shown in Figure 37.

Figure 36.   Brass Weight Attached to Pendulum Arm.
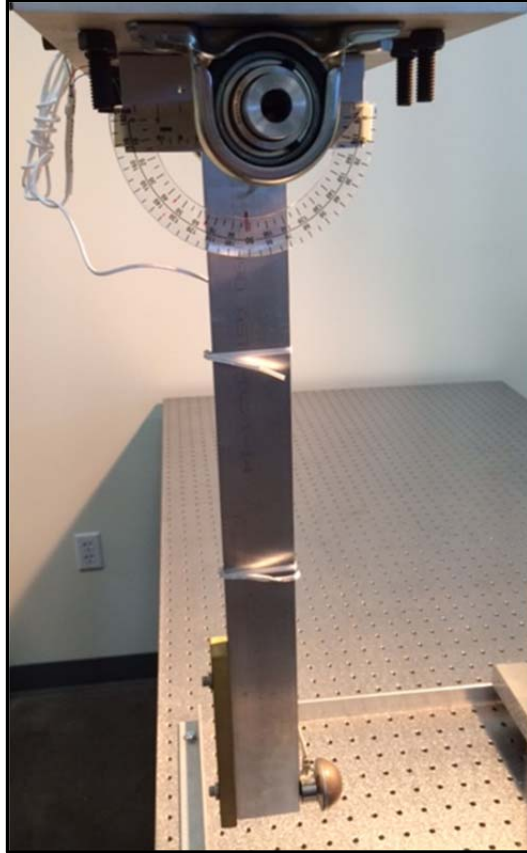
Figure 37.   Complete Impact Pendulum Set-up.

d.   *Impactor*

The impactor was fabricated using a steel hemisphere as depicted in Figure 38, and of the dimensions and properties listed in Table 3 [24].
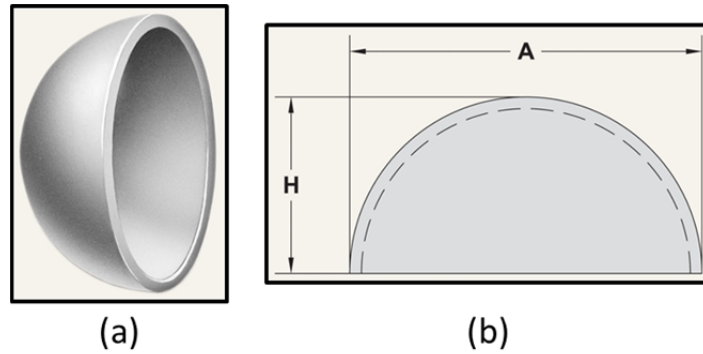
Figure 38.   Steel Hemisphere (a) Isometric View and (b) Side View.
Source: [24].

Table 3.   Steel Hemisphere Dimensions and Material Properties.

Outside Diameter (A)	3.810 cm
Height (H)	1.905 cm
Wall Thickness	3.175 mm
Elastic Modulus	200 GPa
Density	7.87 g/cm^3
Poisson Ratio	0.29

Because the load cell had a threaded connection point, the steel hemisphere was fitted with a threaded insert to attach the hemisphere to the load cell. The insert consisted of 1/4–28 castle nut supported on a plastic sleeve of dimensions, 1.27 cm (long) x 1.429 cm (outer diameter) x 0.953 cm (inner diameter). The plastic sleeve and nut were centered in the steel hemisphere (Figure 39a) and secured with epoxy. When the epoxy was fully cured, the excess epoxy in the nut and sleeve were removed with a drill and tap. The completed impactor had a mass of 36.1 g and is shown in Figure 39b.
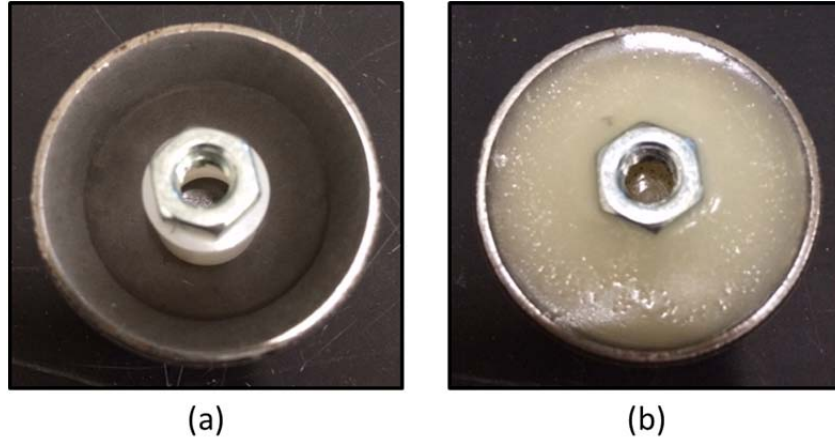
Figure 39.   Impactor Connection (a) Set-up Spacer and Nut
(b) Filled with Epoxy.

2.   Boundary Conditions

The composite structure was fixed between a base plate and top plate for the impact tests. The base plate was fabricated out of 45.72 cm x 45.72 cm x 2.54 cm 6061 aluminum and was considered a fixed boundary. As shown in Figure 40) it was also secured to the table using aluminum angle to prevent any movement. The top plate was fabricated out of 30.48 cm x 30.48 cm x 2.54 cm acrylic glass (PMMA) and was considered a rigid boundary, as shown in Figure 40b. A 5.08 cm hole was drilled into the corner of the top plate to allow for filling and draining the structure. The hole was tapped and could be sealed with a threaded pipe cap. Because the top plate and bottom plate were not connected to each other, the top plate was free to move based on the reaction of the composite structure. Although this was the case, minimal translation of the top plate was possible due to the rigidity of the composite.

To fit the composite structure into the base plate and top plate a groove with a 5 mm width and 1.5 cm depth was machined into both plates. The corners were radius to fit the shape of the composite structure, with the inner corner radius measuring 2.4 mm and the outer corner radius measuring 5 mm. For testing, the composite structure was inserted into the grooves and filled with silicone sealant. To ensure that the fixed boundary in the plates was very secure, 2.5 mm gasket material was pressed into the

groove on the exterior of the composite structure. The structure ready for testing is shown in Figure 41.
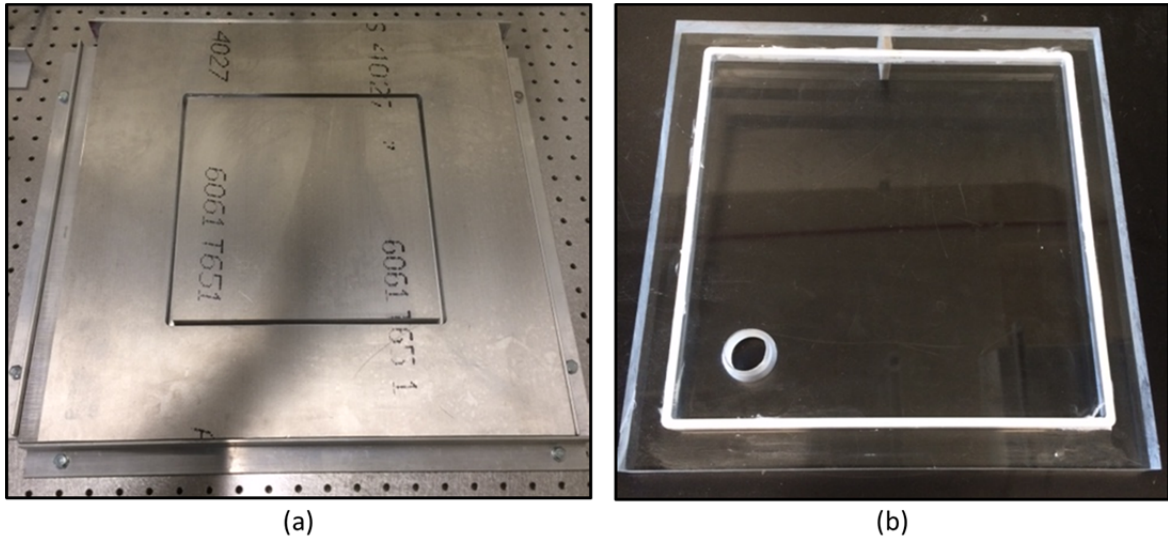
Figure 40.   (a) Aluminum Bottom Plate and (b) PMMA Top Plate.
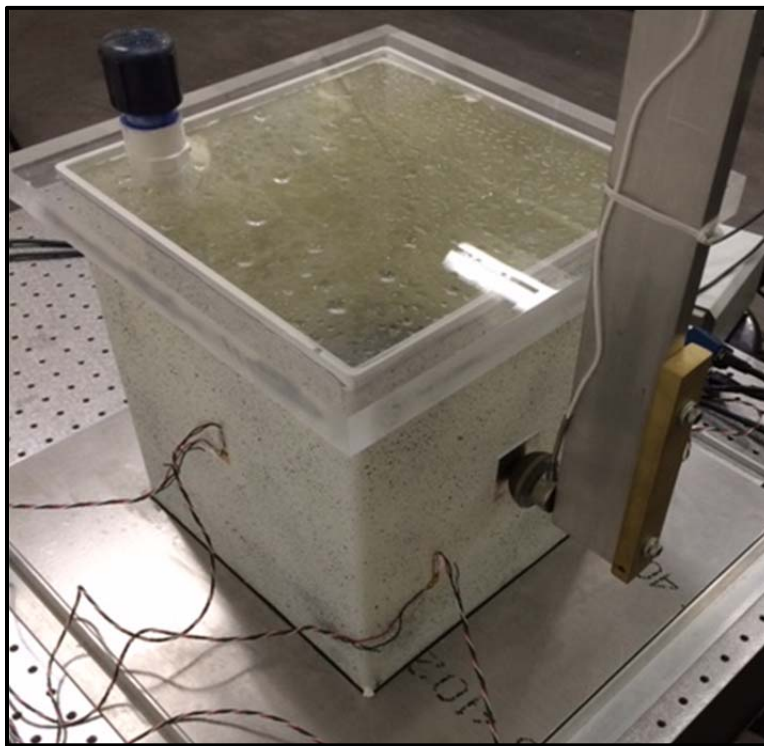
Figure 41.   Complete Experimental Set-up.

3.   Strain Gages

The wired strain gages were connected to a National Instruments ® (NI) 9945 screw terminal adaptors. A screw terminal adaptor was needed for each strain gage direction (x and y axis), totaling eight adaptors. Each of the adaptors was connected to a NI 9237 bridge and strain measurement module via an RJ-50 cable. Additional details on strain gage wiring are included in the Appendix.

4.   Load Cell

The load cell used to measure the impact force was a Honeywell ® Model 31 rated to 2224.1 N [500 lb-f]. It included two threaded connections as shown in Figure 42; one was connected to the end of the pendulum arm and the other connected to the impactor as can be seen in Figure 37 (above). The load cell was connected to a NI 9949 screw terminal adaptor, and like the strain gages, connected to NI 9237 bridge and strain measurement module via an RJ-50 cable. Additional details on strain gage wiring is included in the Appendix.
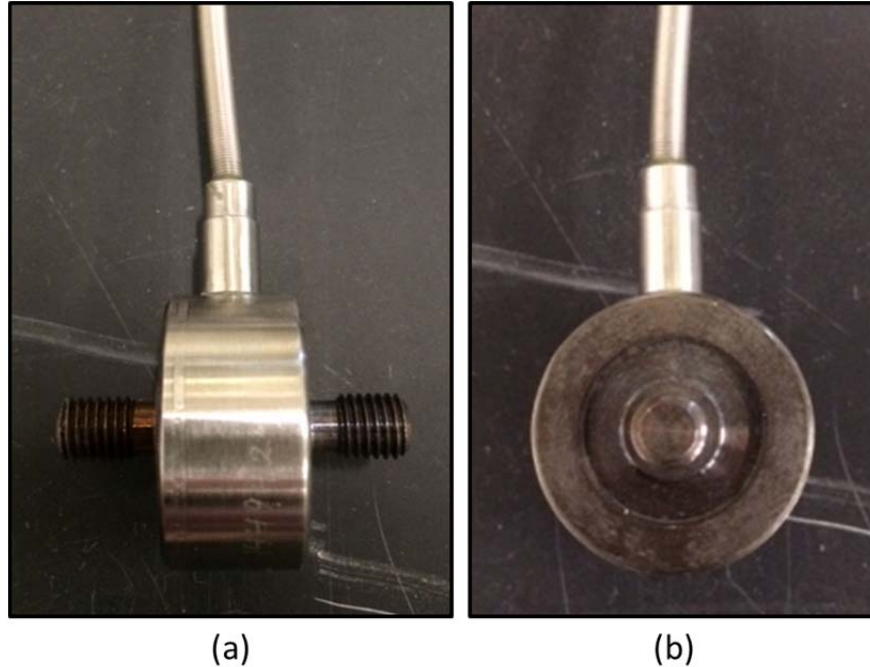
Figure 42.   Load Cell (a) Side View and (b) End View.

5.   Data Acquisition

The strain and impact force data were collected using the NI LabVIEW Signal Express 2012 software suite. The NI 9237 bridge and strain measurement module provided all of the inputs to the data acquisition software simultaneously. The data acquisition time interval was 20 microseconds, allowing for 67,500 samples to be read and recorded for each test run. The full list of software settings is detailed in the Appendix, Table 10.

6.   High-Speed Camera

To capture the deflection of the sides of the composite structure an Olympus® i-Speed 3 high-speed camera fitted with a Nikon® Nikkor 50 mm lens (Figure 43) was used. During testing, the camera was set-up to capture high-speed video of the motion on the front (impact) side and back side. For these videos the camera was located at approximately a 45 degree angle from the respective face. Additionally, the motion of all sides and fluid motion was captured with the camera set-up directly above the structure as

shown in Figure 44. The camera was set to capture the motion of the structure at 1,000 frames per second (fps).

Figure 43.   Olympus® High-Speed Camera, Screen, and Nikon® Lens.
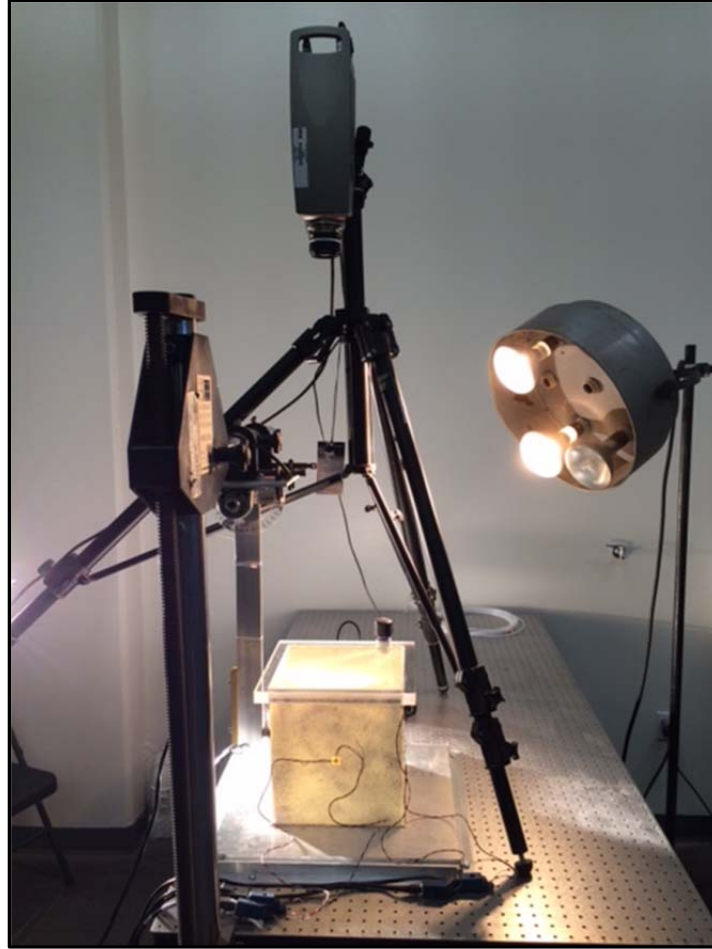
Figure 44.   High-Speed Camera Set-Up for Top-Down Video of Side Movement
and Fluid Propagation.

E.   EXPERIMENTAL METHODS

To test the effects of FSI on the composite structure, tests were conducted with the structure empty (0%), full (100%), and partially filled with water. For each water level the tests were also conducted with various impact forces. The tests for each fill level and impact force combination were conducted with and without baffles installed. Every test was run repeatedly to confirm the consistency of the results.

1.   Fill Level

The composite structure was filled with water incrementally between empty (0%) and full (100%). The additional fill levels that were tested were 25%, 50%, and 75%.

Following some data collection, two additional fill levels (90% and 95%) were added to the analysis in order to fully understand the strain behavior between 75% and 100%.

Because the structure was not transparent, the fill level was determined by volume. In the 100% full condition, the volume was found to be 15980 mL. This was slightly greater than the designed 25 cm cubic volume due to minor variations in the fit to the bottom plate and top plate as well as the radius of the inside corners. In the cases where a baffle was installed the volume was calculated assuming that the foam was solid since it had minimal porosity. The volume associated with each fill level are listed in Table 4.

Table 4.   Fill Level Volumes.

Fill Level	No Baffle	Baffle 1	Baffle 2
25%	3995 mL	3834 mL	3673 mL
50%	7990 mL	7644 mL	7297 mL
75%	11985 mL	11453 mL	10921 mL
90%	14382 mL	13747 mL	13113 mL
95%	15181 mL	14505 mL	13829 mL
100%	15980 mL	15263 mL	14545 mL

2.   Impact

Each fill case was tested with two different impact loads; one with a pendulum drop angle of 25 degrees and the other with a drop angle of 45 degrees. The 25 degree impact corresponded to a 0.959 m/s velocity and the 45 degree impact corresponded to a 1.695 m/s velocity. For the tests, the pendulum was drawn back to the desired angle as read on the protractor and released by hand. It was only allowed to impact the composite structure once; it was caught and its motion stopped as it rebounded. To ensure that the measured results were repeatable and consistent, the test was conducted six times for each drop angle at each fill level. Sufficient time was allowed between each test run for the fluid motion to return to zero.

3. Baffles

The two baffles were inserted in the center of the structure as shown in Figure 45. Both baffles were tested at all fill levels with a drop angle of 45 degrees. As water was added to the structure the baffles floated and were in contact with the top plate for all fill cases (25% through 100%).
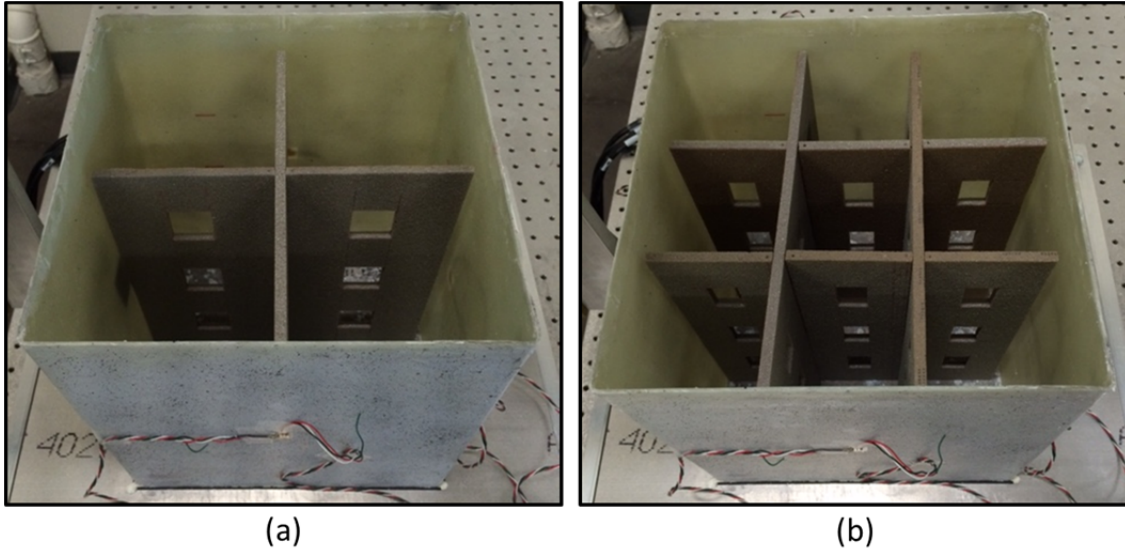
Figure 45.   (a) Baffle 1 and (b) Baffle 2 Installed for Testing.

THIS PAGE INTENTIONALLY LEFT BLANK

III.   RESULTS

A.   IMPACT FORCE ANALYSIS

The impact force for each test was measured over time for comparison between the 25 degree and 45 degree drop angles as well as comparison of the various fill levels. After analyzing the data, high-speed video was used to visually observe and understand the behavior that the data showed.

1.   Impact Force Data

The impact force data was measured for each test run and compared for consistency. For every test, the force data showed incredible repeatability with minimal differences between runs. A representative case of 6 tests (Runs A-F) of a 45 degree impact case are shown in Figure 46.
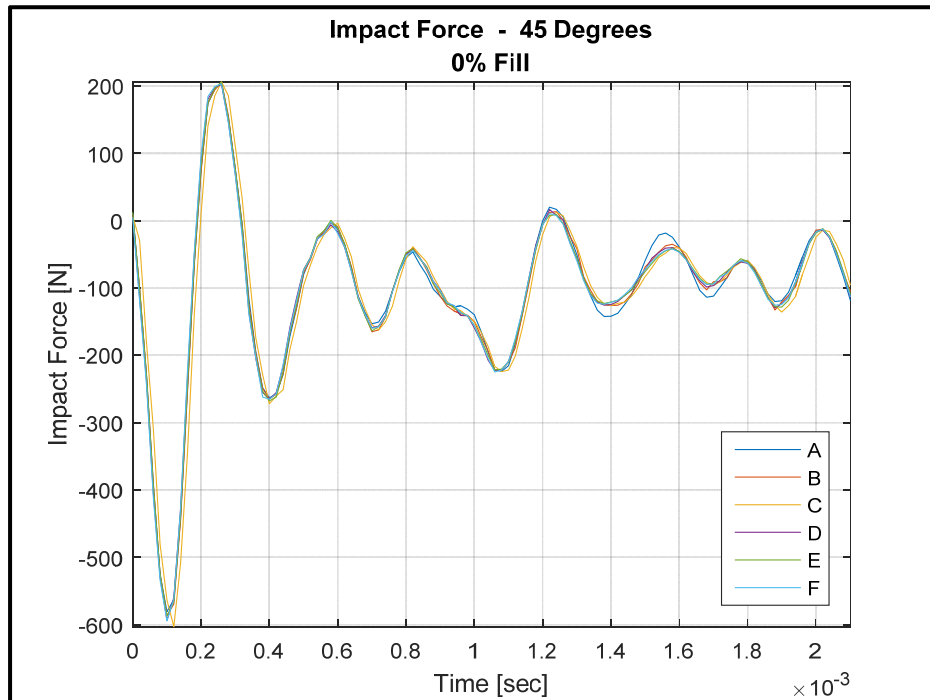
Figure 46.   Comparison of Impact Force Data for 6 Tests.

Due to the consistency of the data, all further figures of the impact force over time will only use one of the test cases. For both the 25 degree and 45 degree drop angles the magnitude of the impact force increased as the fill level increased. At fill levels less than 50% (i.e., 0% and 25%) the magnitudes of the impact force were approximately the same, and at fill levels greater than 50% (i.e., 75%, 90%, 95%, and 100%) they were approximately the same. The magnitude of impact force for the mid fill level (50%) was in between the low fills and high fills, with a slight bias to the low fills. This trend for the 45 degree drop angle is shown in Figure 47 and 48, with the complete set of the high fill levels separated for clarity. The average maximum impact force for all cases are provided in Table 5.
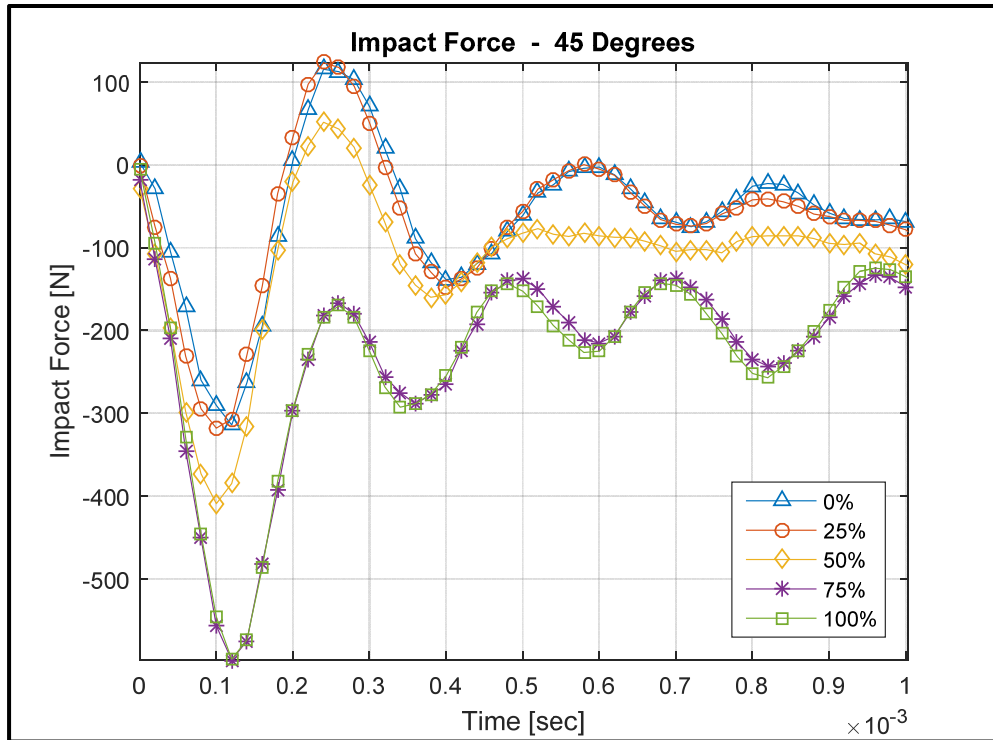
Figure 47.   Plot of Impact Force Versus Time.
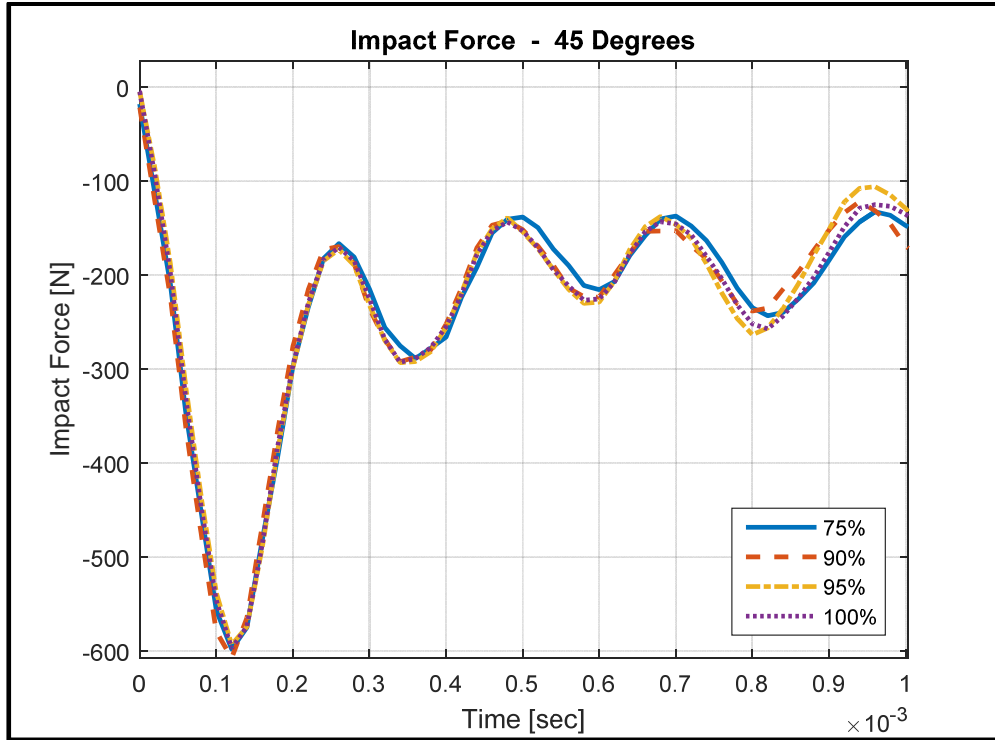
Figure 48.   Plot of Impact Force Versus Time for High Fill Levels.

Table 5.   Average Maximum Impact Force.

Fill Level	Maximum Force (25 Degrees) [N]	Maximum Force (45 Degrees) [N]
0%	315.5	590.9
25%	317.6	593.5
50%	417.2	772.5
75%	603.4	1130.5
90%	604.9	1127.2
95%	594.0	1121.2
100%	599.2	1117.6

For each of the impacts, regardless of the drop angle, the force was oscillatory before returning to zero. It is important to note that the force data could also be oscillatory when the load cell was barely moving. Because the load cell determined force based on acceleration, the period of time that the force was oscillatory after reaching a maximum occurred because the cell was moving within its housing. After the initial impact and maximum force, the impactor experienced a period of time where it remained in contact with the structure before rebounding. The behavior after the initial contact

varied with the fill level. For the low fill cases (<50%), the impactor made initial contact with the structure, remained in contact with the structure for a period of time, and then rebounded. For the mid and high fill cases (50% and greater), the impactor made initial contact with the structure and then experienced additional impacts before rebounding. These additional impacts can be seen in Figures 49 and 50 as the negative spikes after the initial maximum force. Also of note is the amount of time that the impact force is non-zero, indicating contact with the structure. For all cases, the maximum impact force occurred at 1.0 to 1.2 msec, but the total amount of the time that the impactor was in contact with the structure increased as the fill level increased. The approximate values of the contact time for the various fill levels are listed in Table 6.
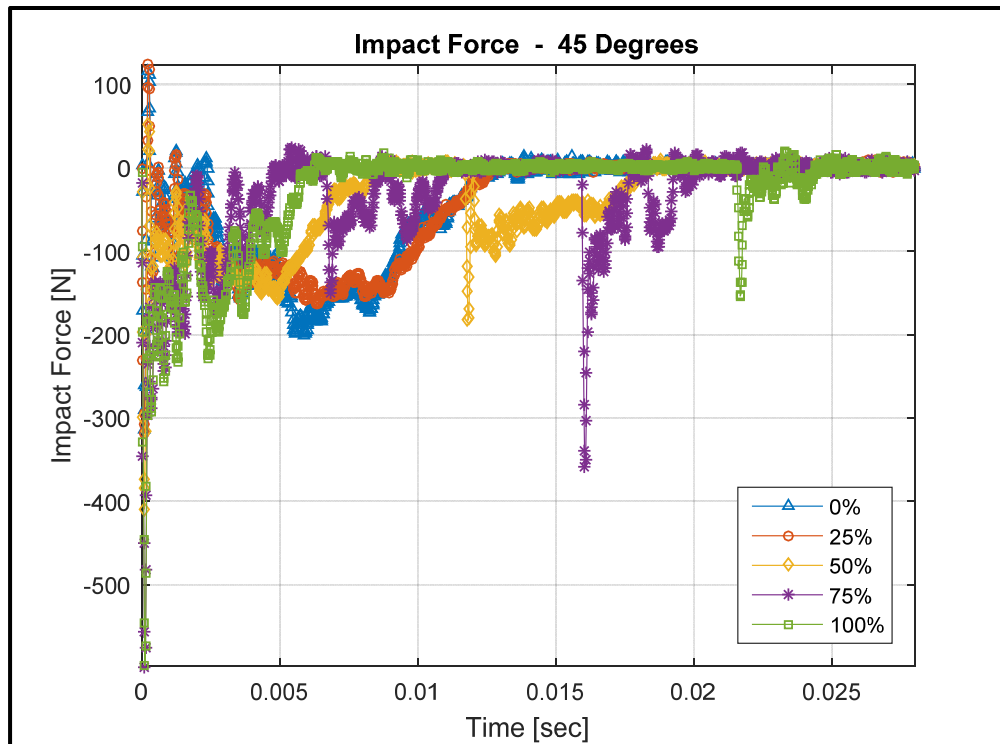
Figure 49.   Additional Impactor Contact with Structure.
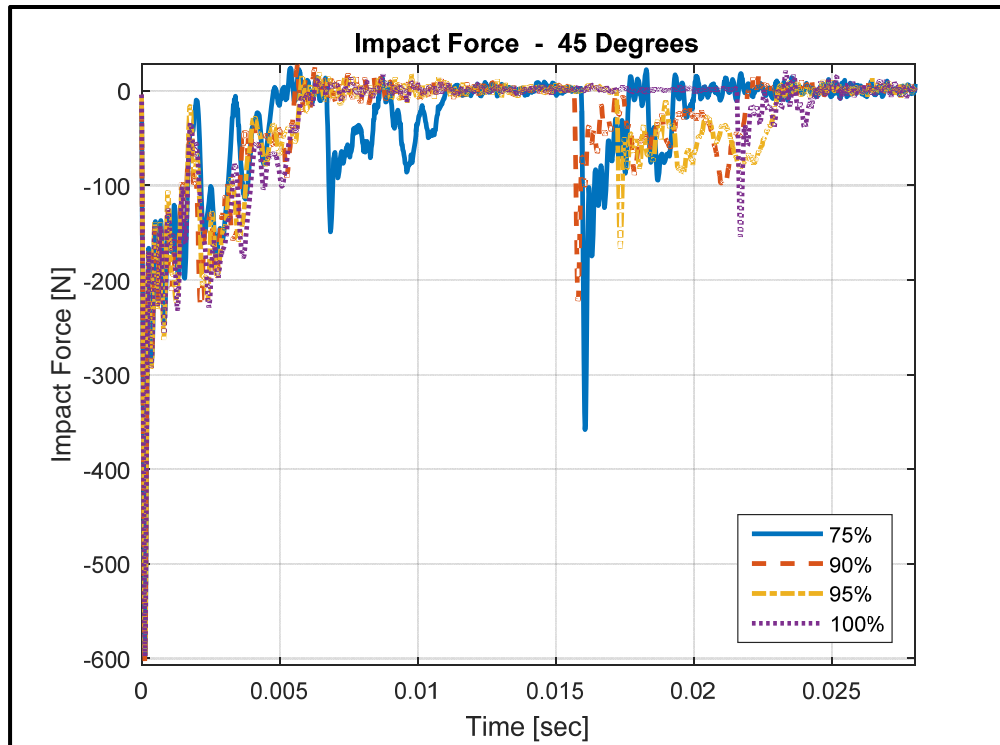
Figure 50.   Additional Impactor Contact with Structure (high fills).

Table 6.   Impactor Contact Time with Structure.

Fill Level	Contact Time [msec]
0%	13
25%	13
50%	18
75%	21
90%	22
95%	22
100%	25

2.   Impact Force Trends

To best understand the trend of the maximum impact force with respect to the fill level the average maximum force with standard deviation was plotted (Figure 51). The trend showed that with great consistency the low fill levels and high fill levels were comparable in magnitude with a transition occurring at the mid fill level. These differences are attributed to the added mass effect that was present in the structure when water was added. For comparison, the tests that included a baffle were also plotted. The

51

results had minor differences from the tests without a baffle. For all fill levels, the average maximum force for Baffle 2 is slightly less than that of Baffle 1, and both are less than those without a baffle. These minor differences are due to differences in fluid mass contained in the structure. For each fill level the volume of water differed in the baffle cases due to the volume of the foam present (Table 4). Thus, with less water there was less mass resulting in a slightly lower maximum force.
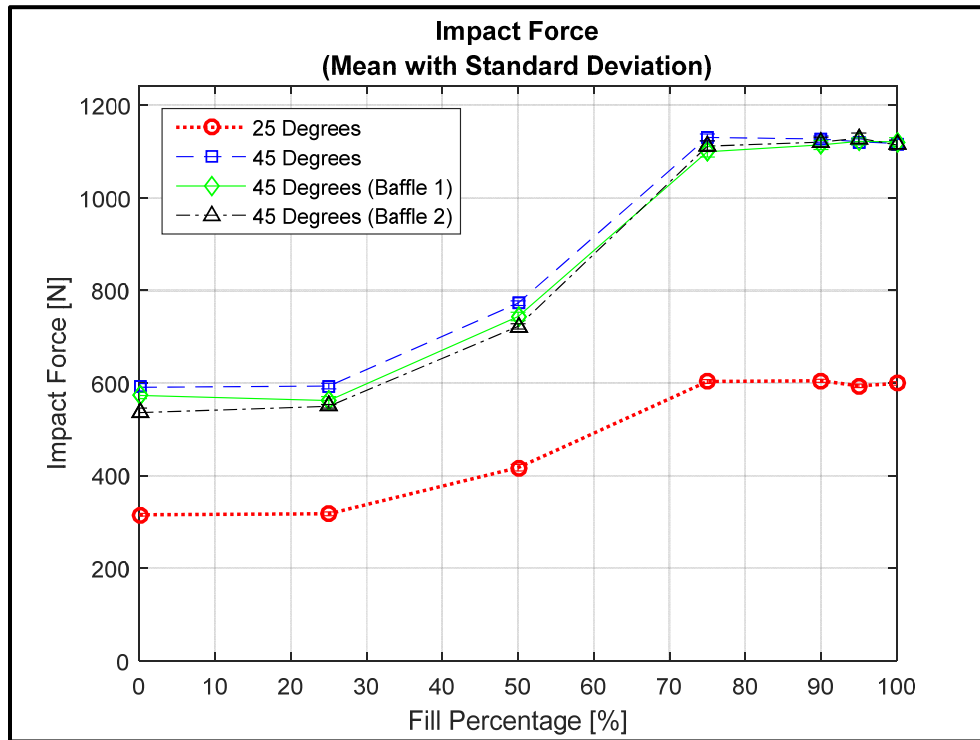
Figure 51.   Impact Force Trend for Various Fill Levels.

3.   Visual Observation

With the high-speed camera images, the impact behavior was studied for each fill level. The difference in the responses was very apparent in the low, mid, and high fill cases. A representative example of a high-speed camera image at impact is shown in Figure 52. In the low fill cases, the impactor made contact with the structure, both moved inward to a point of maximum deflection, and then moved outward together until the impactor separated from the structure. It followed the shape expected for the first mode of a clamped plate. For the mid and high fill levels the impactor made contact with the

52

structure, momentarily paused while the structure oscillated, and then rebounded, separating from the structure. During the period of time that the structure was oscillating, multiple additional contacts were made between the impactor and structure. The motion could best be described as the structure "rattling" on the impactor before separation finally occurred. Although the exact mode shape could not be seen, the motion of the structure after impact at the mid and high fill levels was a higher mode than that of the low fill levels. The 100% fill level was slightly different from the other high fill levels. The mode shape was not exactly like the empty condition but the structure deformed inward and then reversed direction. The structure and the impactor separated during the time of maximum deflection and re-contacted prior to the impactor rebounding.
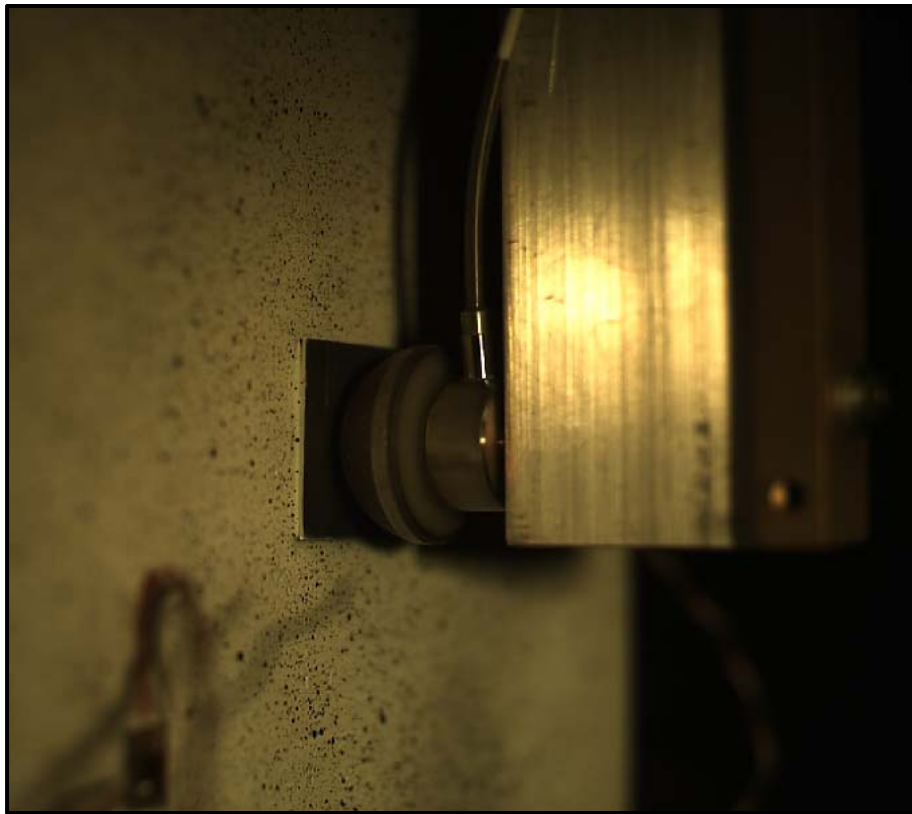
Figure 52.   High-Speed Camera Image of Impact for 25% Fill Level.

B.   STRAIN ANALYSIS

The strain response was measured for each side simultaneously beginning with the impact, and was recorded for a 70 msec period. Both the horizontal (x-direction) and vertical (y-direction) components of strain were measured but all discussion of results refers to the horizontal components unless otherwise mentioned.

1.   Strain Versus Time Data

Like the impact force data, the strain response was measured for each test run and compared for consistency. For each test, the strain response data also showed incredible repeatability between runs regardless of the side or fill level. Representative cases of 6 tests (Runs A-F) are shown in Figure 53 for a 45 degree impact with low fill (0% fill) for the front side; a 45 degree impact with high fill (75% fill) for the back side is shown in Figure 54. Due to the consistency of the data, all further figures of the strain over time will only use one of the test cases.

Figure 53.   Comparison of Strain Response Data for 6 Tests (0% fill).

Figure 54.   Comparison of Strain Response Data for 6 Tests (75% fill).

a. Front Side

On the front side, the response of the structure differed among the fill levels after the initial contact of the impactor. For the low fill cases (0% and 25%) the strain started as positive (tension) as the impactor moved into the structure. It then shifted to negative (compression) as the structure moved 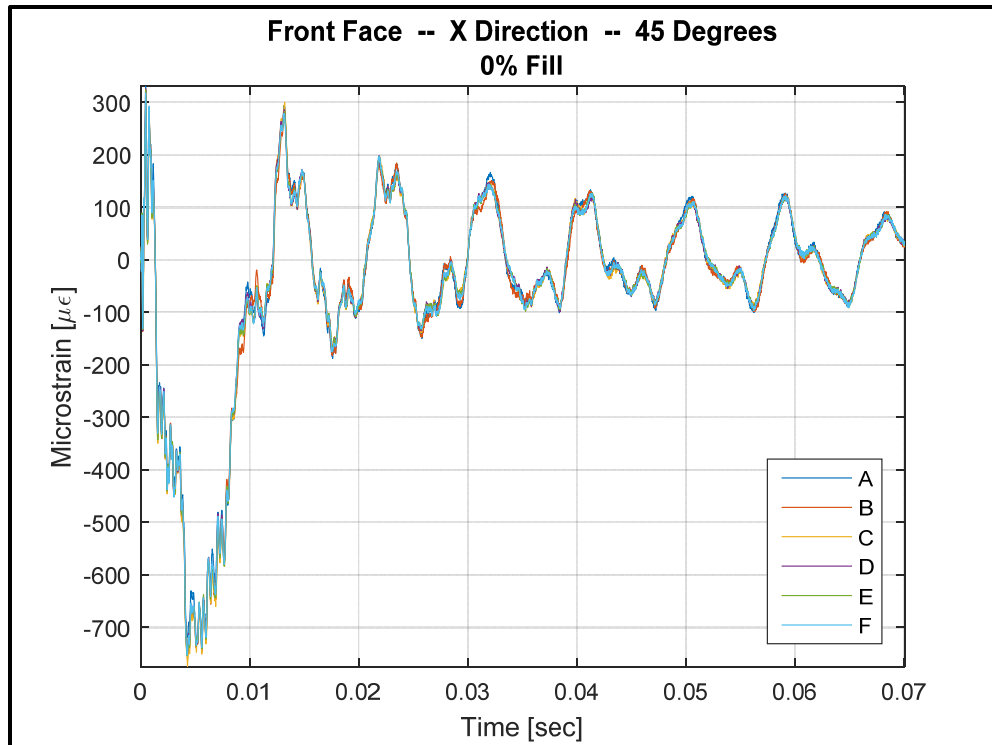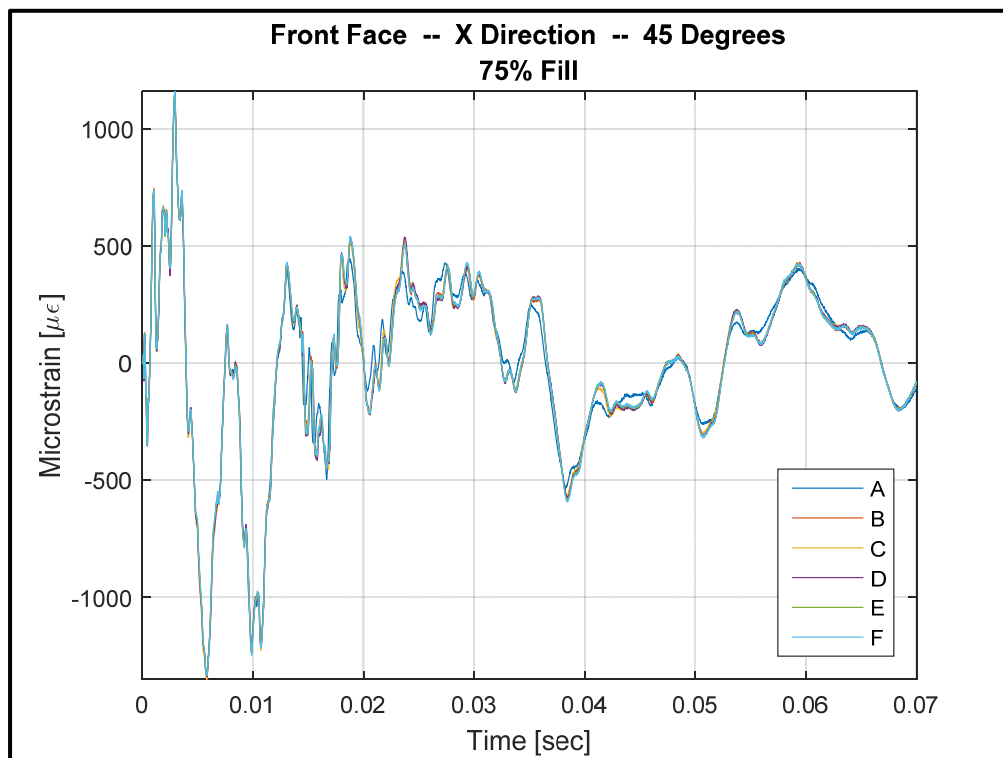to the maximum inward deflection and finally returned to positive as the impactor separated from contact. In both low fill cases, the maximum strain value was negative and occurred at the point of maximum deflection. In the high fill cases (75%, 90%, 95%, and 100%), the opposite initial strain response occurred. The strain started as positive as the impactor moved into the structure and then shifted to negative during the time that the impactor was in contact with the structure. As the impactor separated from contact, the strain returned to positive and began to decay over time. In all of high fill cases with the exception of 100% fill, the maximum strain values were negative. In the full condition (100%), the maximum strain occurred in tension. For the mid fill level (50%) the strain behavior followed the characteristics of the both the low and high fill levels. The strain started as negative, as was seen in the high fill cases, but the magnitude did not reach a similar level for the first positive peak. As the strain transitioned back to negative, it followed an oscillatory pattern as was seen in the high fill cases but had a greater positive magnitude at the time that the impactor separated contact. Like the majority of the other fill cases, the maximum strain occurred in tension. Plots of the strain response for the front side are shown in Figures 55 through 57. For clarity, the high fill cases are plotted separately.

Figure 55.   Strain-Time History for the Front Side (zoom).

Figure 56.   Strain-Time History for the Front Side.

Figure 57.   Strain-Time History for the Front Side (high fill).

As the fill level was increased, the absolute maximum strain also increased. In the high fill levels, the maximum strain occurred between 75% fill and 95% fill, with the maximum depending on the drop angle and presence of a baffle. In all conditions the maximum strain for the full (100%) case was less than the other high fill cases (75%, 90%, and 95%). The trend of the front side absolute maximum strain across all fill levels was consistent for all conditions regardless of the drop angle and presence of a baffle. The strain trend for the front side is shown in Figure 58.
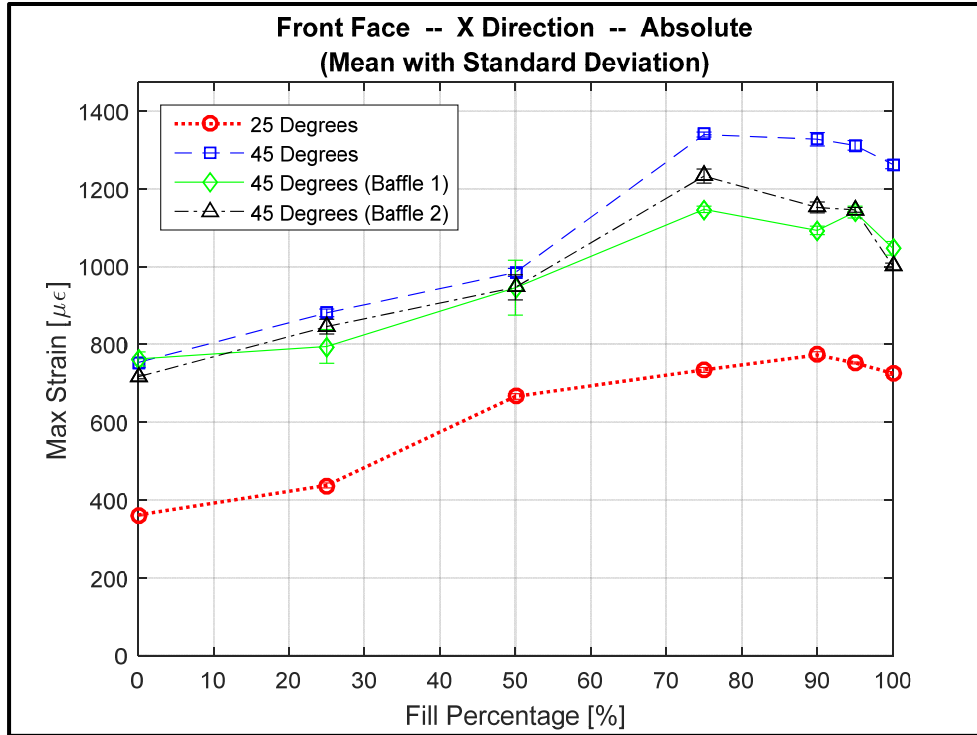
Figure 58.   Absolute Maximum Strain Trend Across Fill Levels (front side).

b.   *Left / Right Side*

The left and right sides showed strain behavior that was very similar over time with slight variations in magnitude. The differences in magnitude are attributed to the minor differences in thickness for the two sides. For both the left and right sides, the strain over time was predominantly in tension and the maximum strain occurred in tension for all fill levels. This differed from the front side in which the strain oscillated evenly between tension and compression over time, and the maximum strain for every case but 100% occurred in compression.

The time to the maximum strain generally increased with the fill level. There was a slight increase among the low fill levels, and the largest increase occurred between the 50% fill and 75% fill. The higher fills saw a slight decrease for the time to the maximum strain as they actually occurred earlier than that of the 75% case. The strain time history for the left and right sides are shown in Figures 59 through 62. For clarity, the high fill cases are plotted separately.

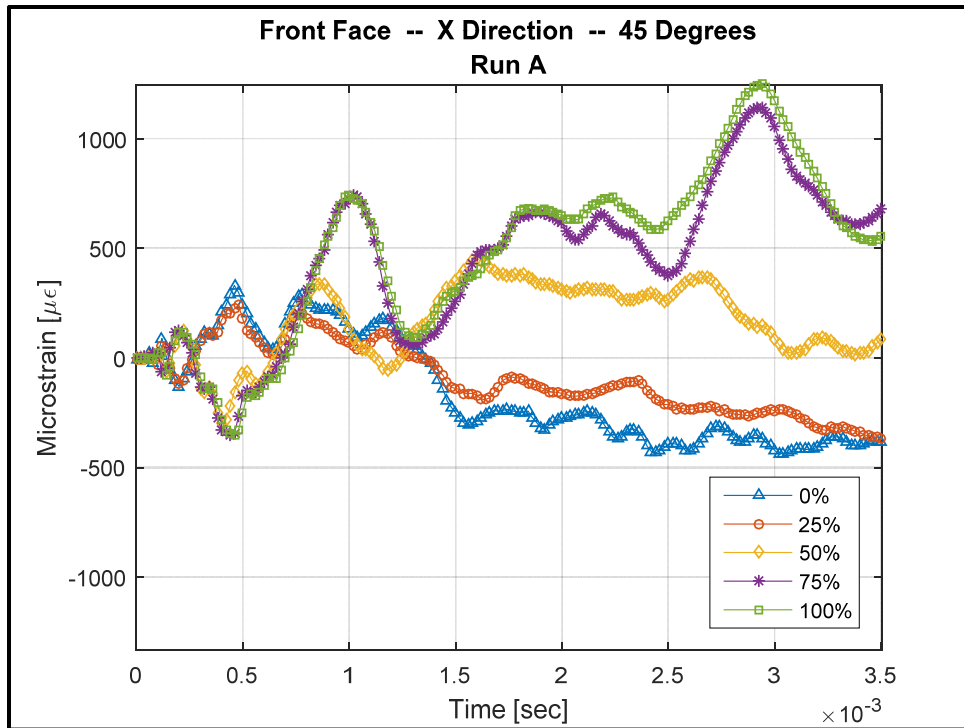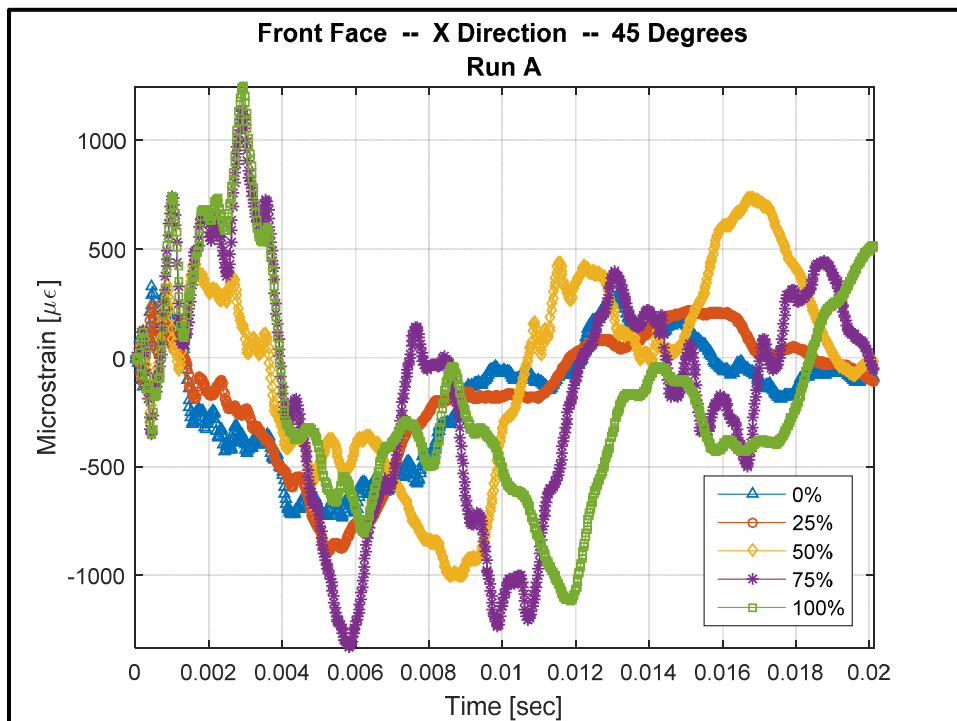Figure 59.   Strain-Time History for the Left Side.
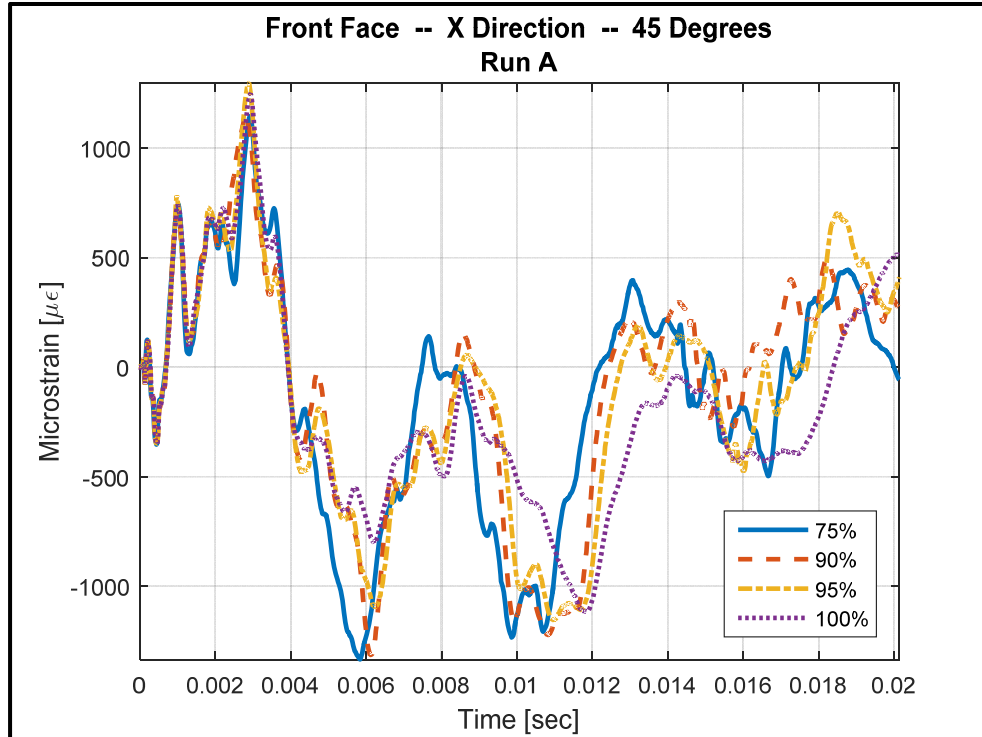

Figure 60.   Strain-Time History for the Left Side (high fill).

Figure 61.   Strain-Time History for the Right Side.
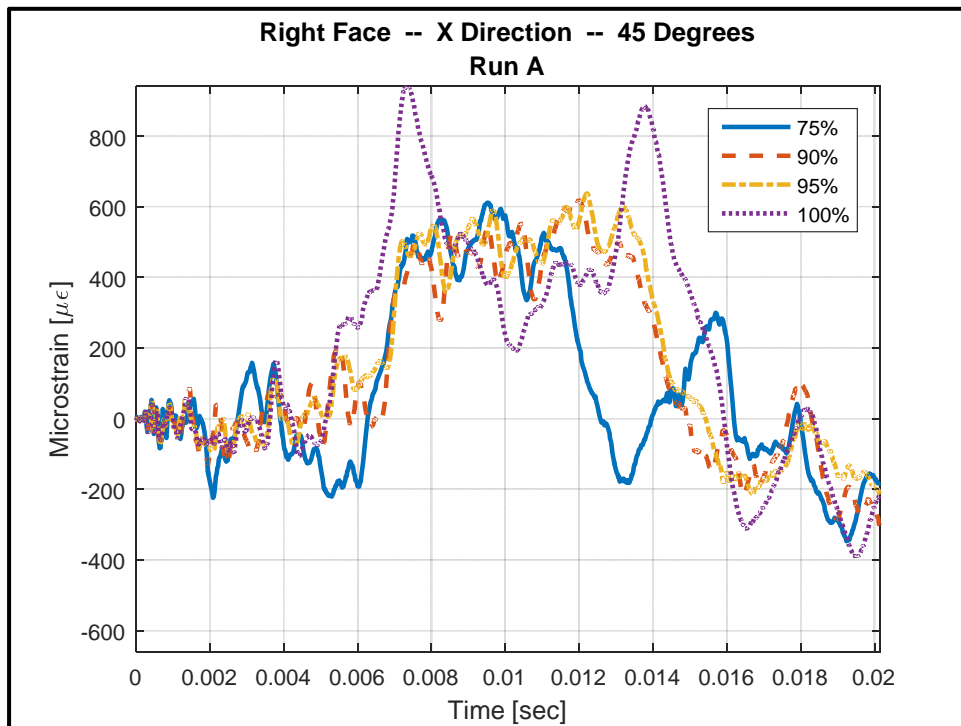
Figure 62.   Strain-Time History for the Right Side (high fill).

61

The strain trend across the various fill levels differed from that of the front face. The maximum strain decreased from 0% fill to 25% fill, followed an increase to 75% fill. There was a very slight decrease in the maximum strain between the 75% fill and 90% fill, but the remaining high fill levels showed an increase in strain magnitude. The full (100%) case was the maximum strain for both sides. The trends of both the left and right sides for the 25 degree and 45 degree drop angles are shown in Figure 63. As previously discussed, the differences in magnitude are attributed to the variation in the side thicknesses, but the trends are almost identical. Also, the trend of the maximum strain across the fill levels is not affected by the impact force (drop angle).

The effect of the baffles on the left and right side strains is shown in Figure 64. The results varied somewhat between the sides, and both sides were inconsistent as to the effect of a baffle. The left side was more consistent and in almost every case with a baffle, the strain was reduced. The right side showed some instances of reduced strain but not in the majority of cases.
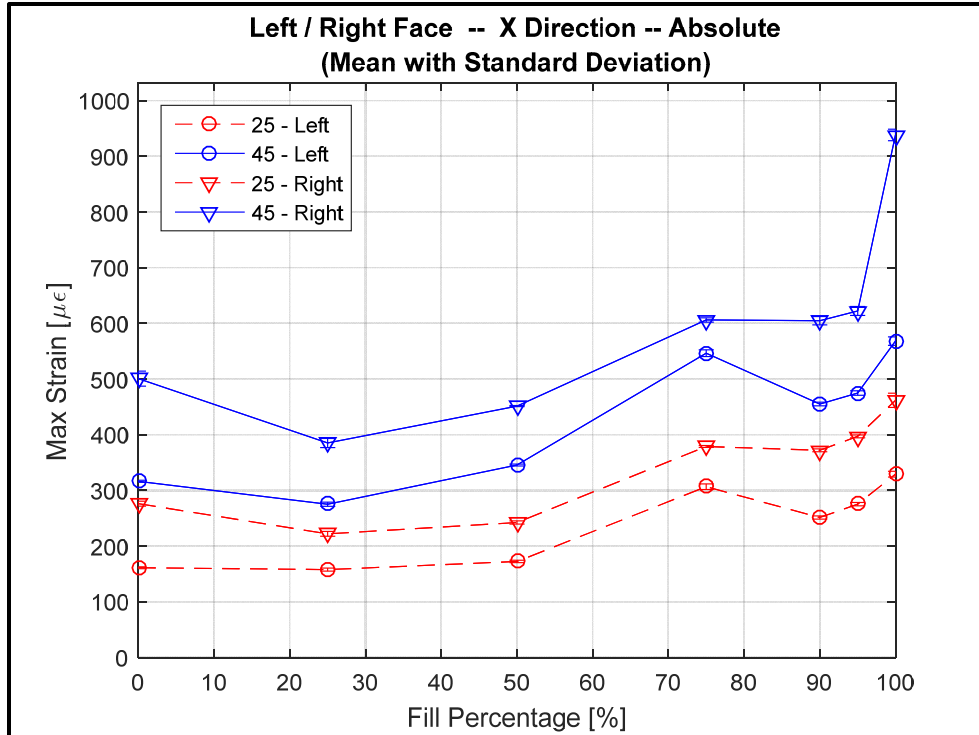
Figure 63.   Absolute Maximum Strain Trend Across Fill Levels (left/right side).
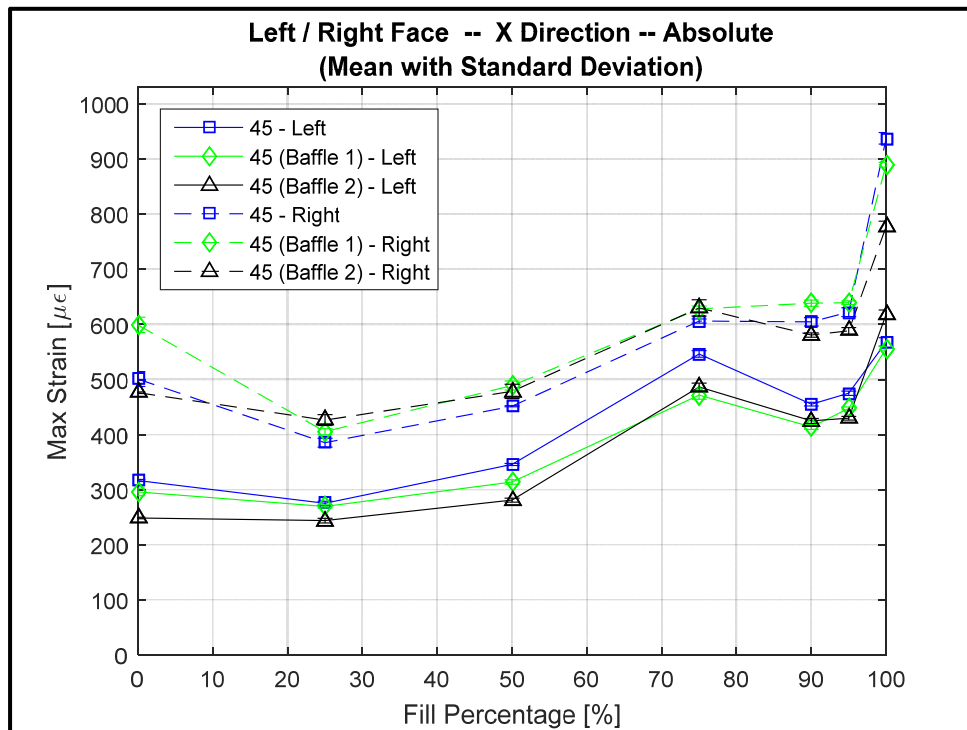
Figure 64.   Absolute Maximum Strain Trend Across Fill Levels (baffles).

63

c.   Back Side

The strain behavior on the back side showed a similar oscillatory pattern as the left and right sides but started later, as the effects of the impact moved around the structure. For all fill levels, the strain variation was minimal for approximately 3 milliseconds after the impact. The strain on the back side was also predominately in tension and all maximum strains occurred in tension. The strain time history for the back side is shown in Figures 65 and 66. For clarity, the high fill cases are plotted separately.
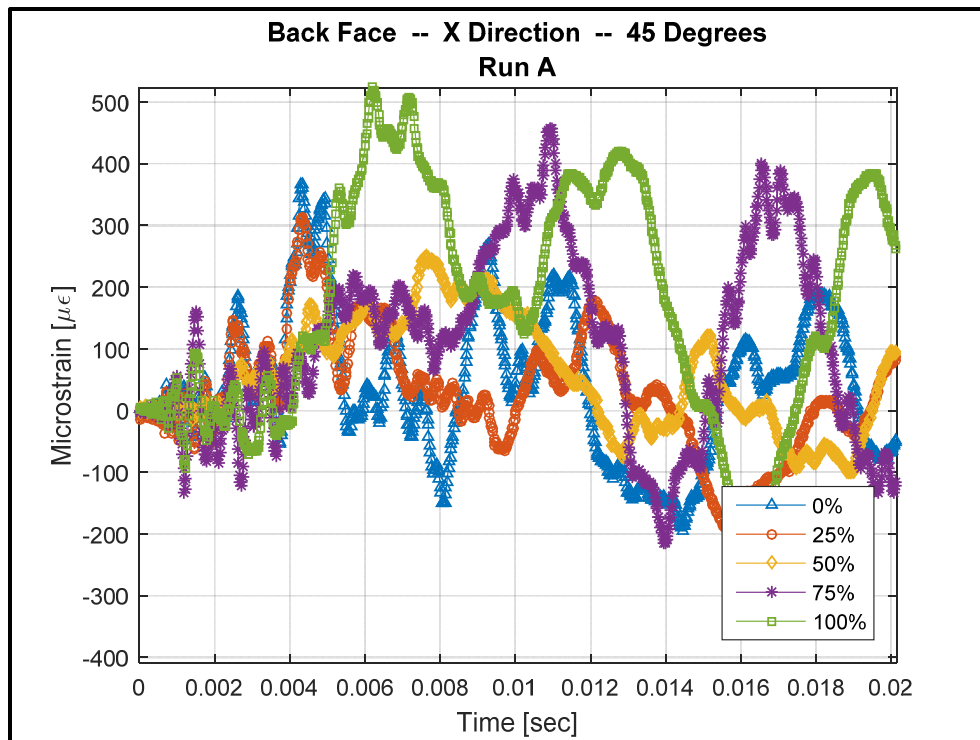
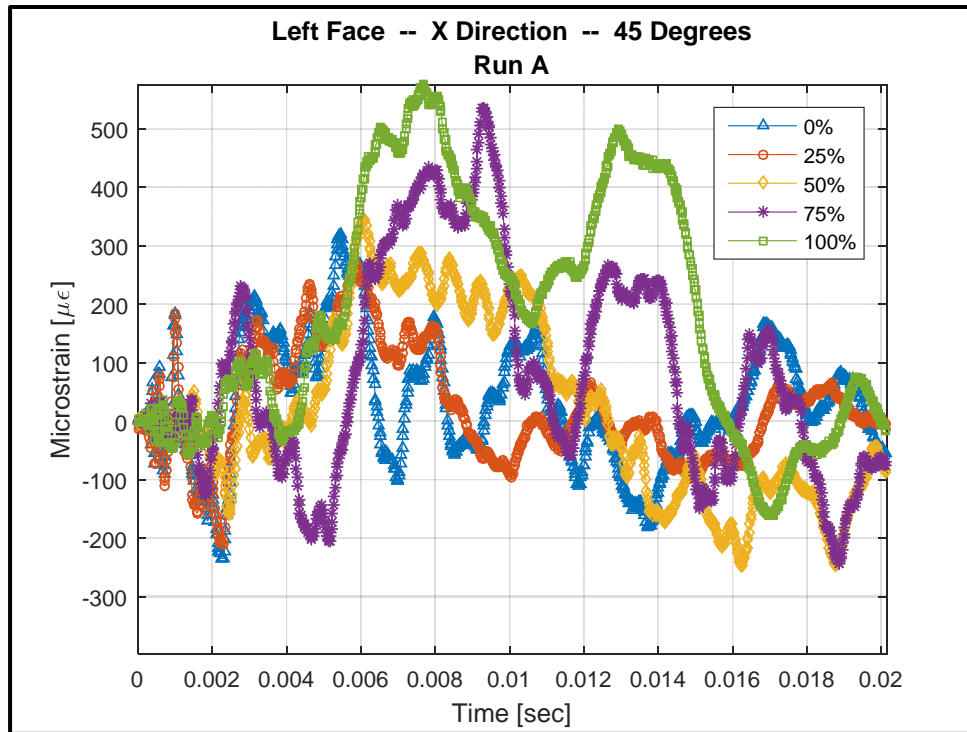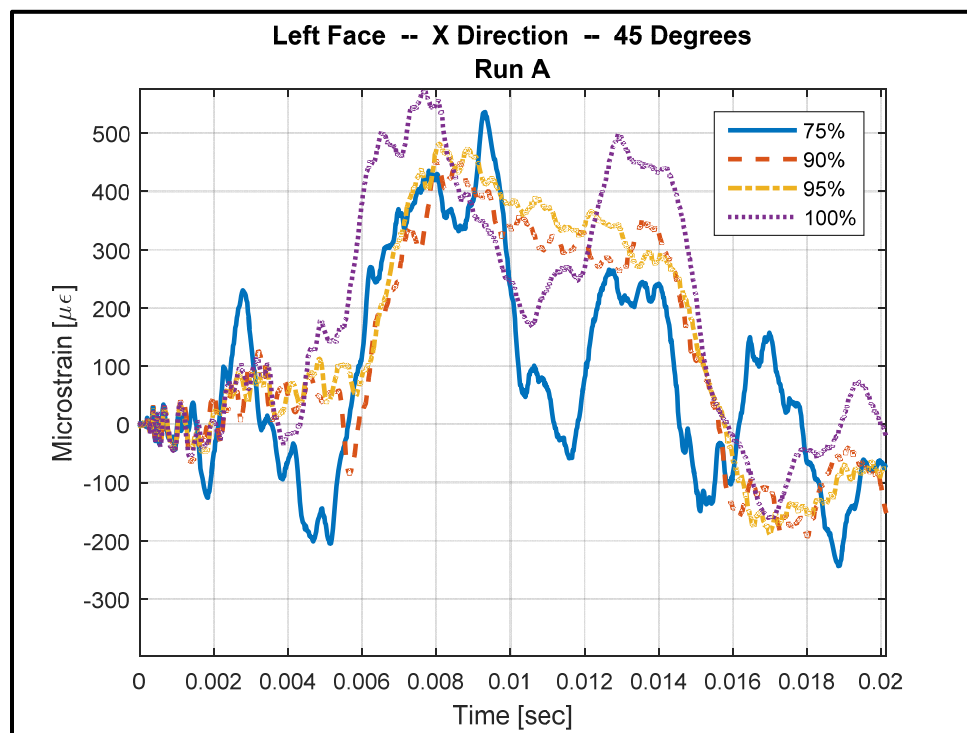Figure 65.   Strain-Time History for Back Side.
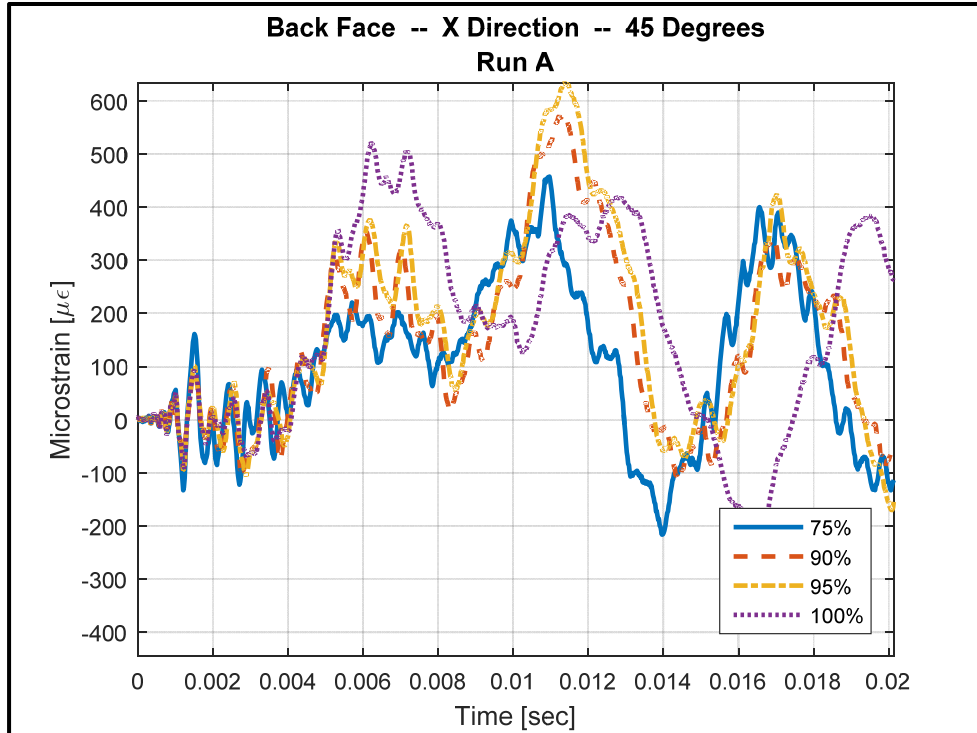
Figure 66.   Strain-Time History for Back Side (high fill).
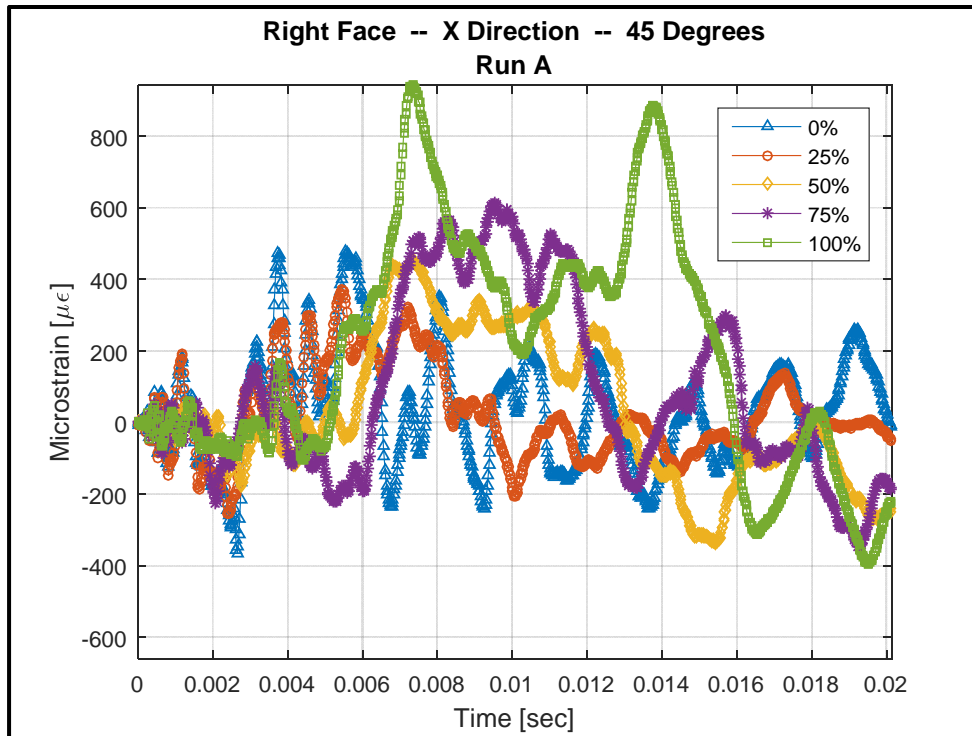
As the fill level was increased, the maximum strain generally decreased for the low fill cases and increased in the high fill cases with a transition occurring at the mid fill level. The 50% case had the smallest strain, and the strain increased until it reached a maximum at the 95% case. The magnitude of the maximum strain was more than doubled between 50% and 95%. The maximum strain then decreased in the 100% fill case. This was the characteristic trend for both the 25 degree and 45 degree drop angles. It was also true in the cases that included a baffle. The standard deviation for the maximum strain was also plotted and was noticed to be the greatest for the 50% fill case; at this fill the standard deviation on the back side was also greater than the front, left, and right sides. The maximum strain magnitude on the back side as function of fill level is shown in Figure 67.
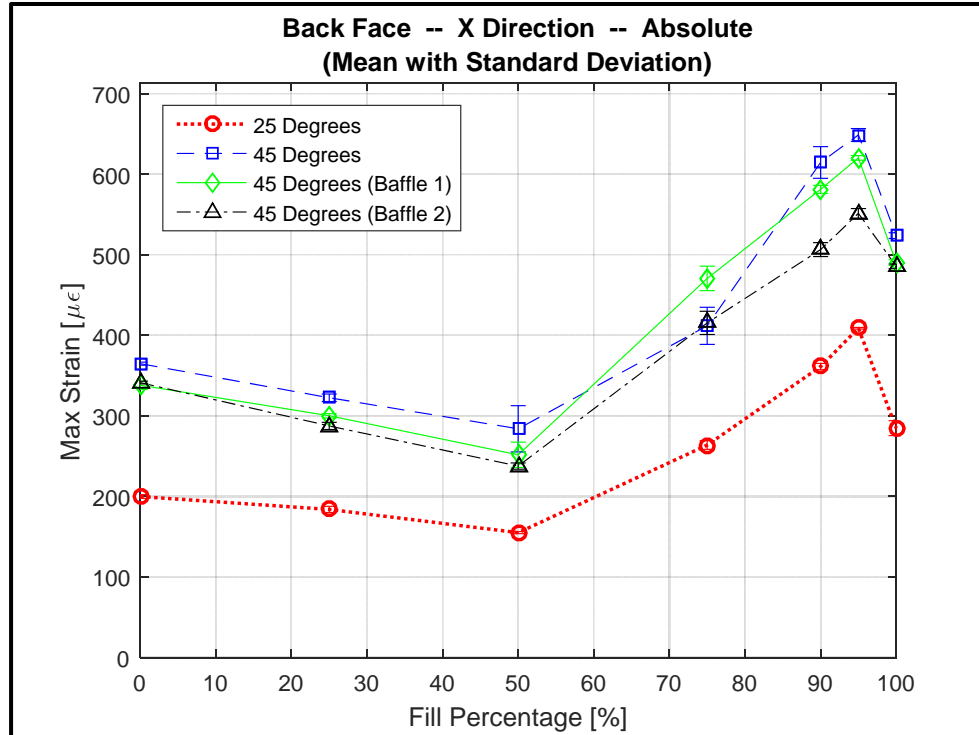
Figure 67.　Absolute Maximum Strain Trend Across Fill Levels (back side).

The amount of time to the maximum strain on the back side was also plotted as function of the fill level, as shown in Figure 68. In general, the time to the maximum strain increased as the fill level increased. The 0%, 25%, and 100% fill cases had approximately the same values as the maximum strain occurred on the first major peak and then began to decay over time (Figure 65). For the high fill cases, less 100%, the time that it took for the strain to build was greater and the maximum strain occurred on the second major peak (Figure 66). The mid fill case did not have a peak strain that was as sharp as the other fill cases and had a large standard deviation among its values. Two alternative situations occurred for the various test runs at 50%. In one case, the maximum strain was on the first major peak in tension and in the other case the maximum strain was on the second major peak in compression. This phenomenon can be seen in Figure 69. Of note, the absolute magnitudes of the maximum strains are approximately the same. In order to validate that this behavior was repeatable, the number of test runs for the 50% fill case were increased from 6 to 18. In 9 out of the 18 tests, the first case occurred where the maximum strain was in tension, and in the other 9 tests, the second case

66

occurred where the maximum strain was in compression. To further confirm this phenomenon, the fill level was increased to 55% and 60%, the same behavior persisted. It was apparent that this bifurcation was consistently present at the mid fill level for the 45 degree drop angle. Additional analysis was conducted of the high-speed video and frequencies of the strain-time data for back side. These results are discussed in the next sections.
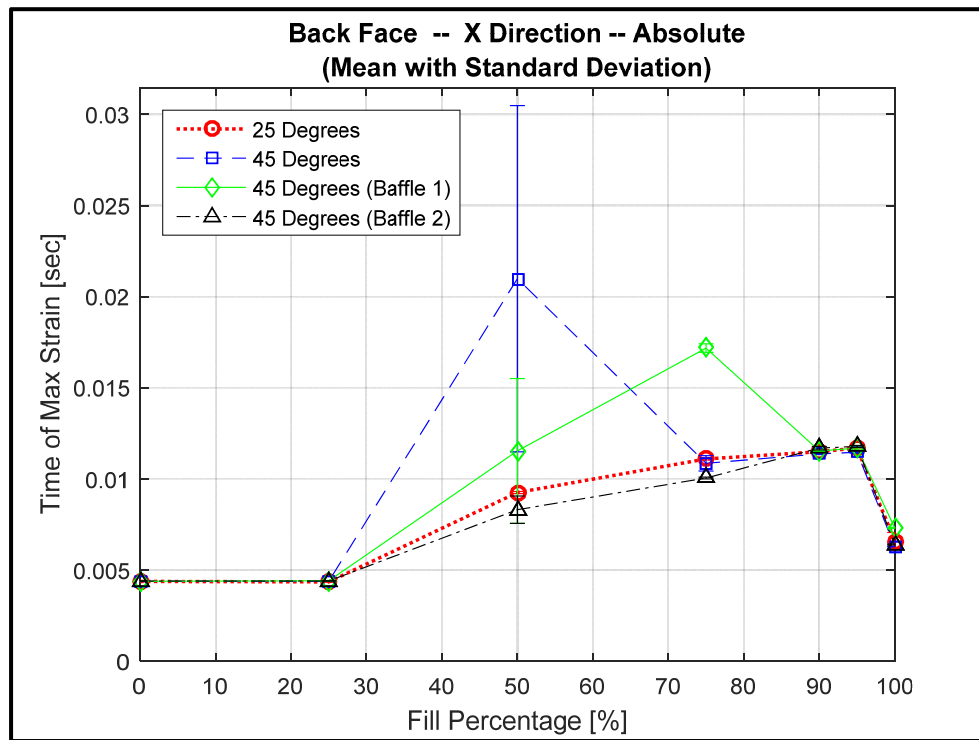
Figure 68.   Time of Absolute Maximum Strain Across Fill Levels (back side).
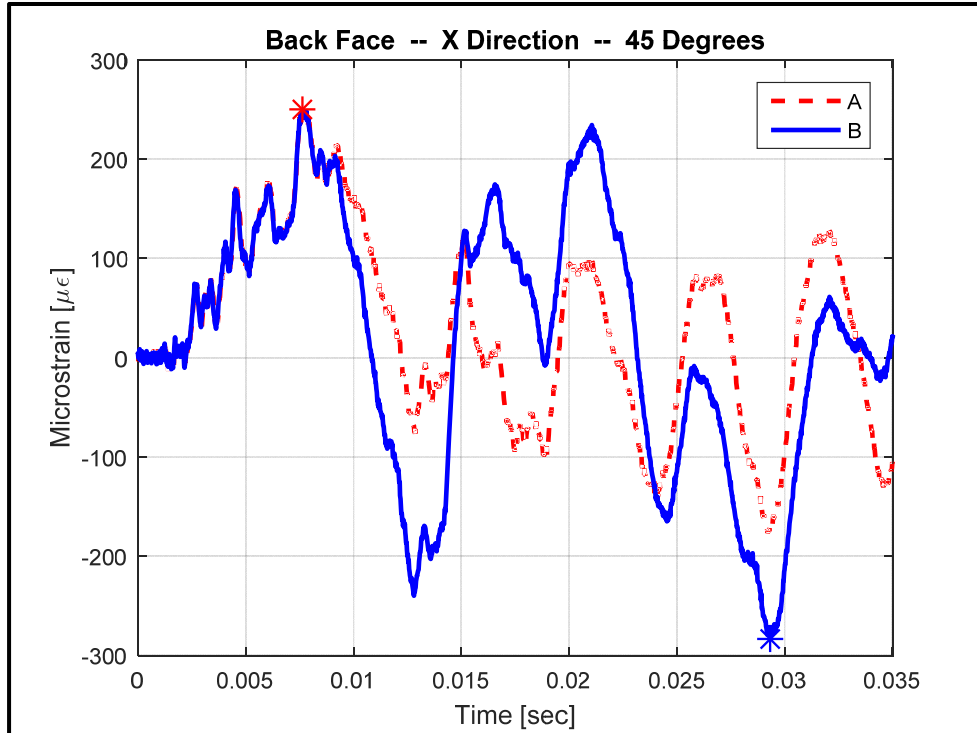
Figure 69.   Strain-Time History for Back Side (50%).

As was the case for the front, left, and right sides, the strain on the back side was approximately doubled between the 25 degree impact and the 45 degree impact. Similar to the front side, the baffles reduced the strain, especially in the high fill cases. As the fill level was increased, so was the effect of baffle on reducing the strain. This can be seen in Figure 67 (above) as the difference in the strain magnitude increased above 50% fill. The greatest reduction in strain on the back face occurred at the 95% fill level. In this case, Baffle 1 reduced the maximum strain by approximately 3% while Baffle 2 reduced the strain by approximately 13%. The effects of the baffles on the strain are shown in Figure 70.

Each baffle did not have the same effect on the bifurcation phenomenon at the mid fill level. Baffle 2 eliminated the bifurcation while it remained with Baffle 1.
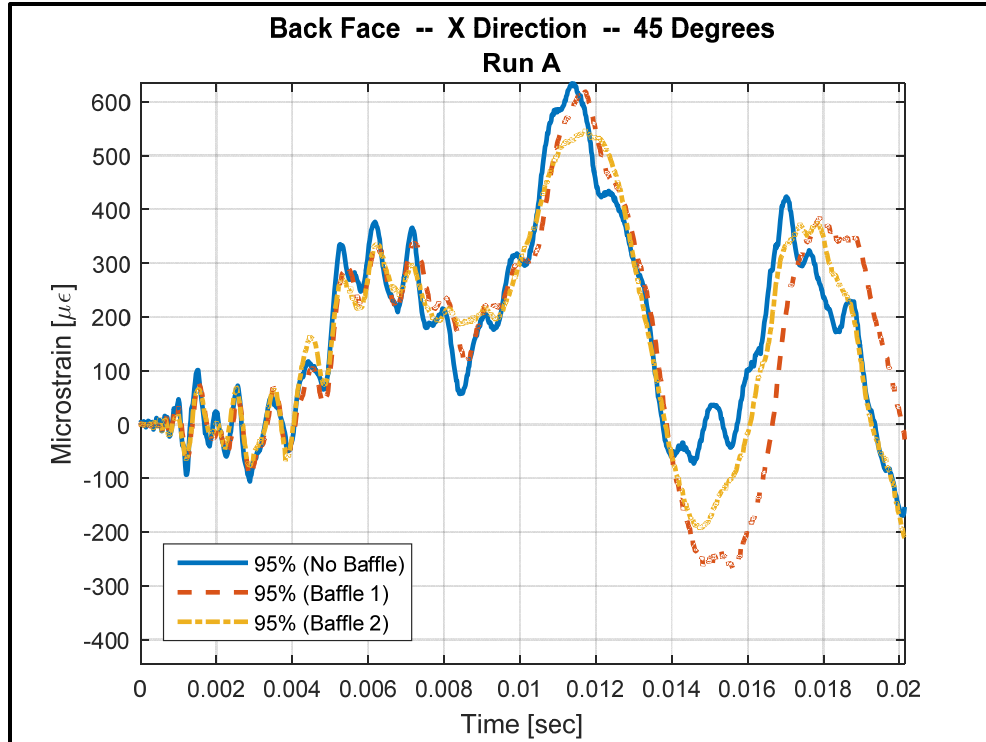
Figure 70.   Strain-Time History for Back Side (baffles).

2.   Visual Observation

Similar to the front side, high-speed video was used to observe the structural response of the back side of the composite for the various fill cases. The camera was also positioned directly above the structure so that the response of all sides could be observed as well as the fluid motion.

a.   *Back Side*

The high-speed video allowed for a qualitative comparison of the structural response at the various fill levels. An image from the high-speed video is shown in Figure 71. Although the exact mode shape could not be determined, there was an obvious difference in the low fill, mid fill, and high fill cases. In the low fill cases, the structure deformed outward at the center and oscillated in an inward to outward motion like a plate in first mode bending. In the high fill cases, the structure deformed outward at the top and inward at the bottom. It behaved as would be expected in second mode plate bending but there were also elements of first mode behavior present. For the mid fill case, the

69

distinction between the two mode shapes was more difficult to distinguish. The motion appeared to be a combination of the first and second modes of plate bending. The bifurcation that was present in the strain data was not clearly apparent from visual observation.
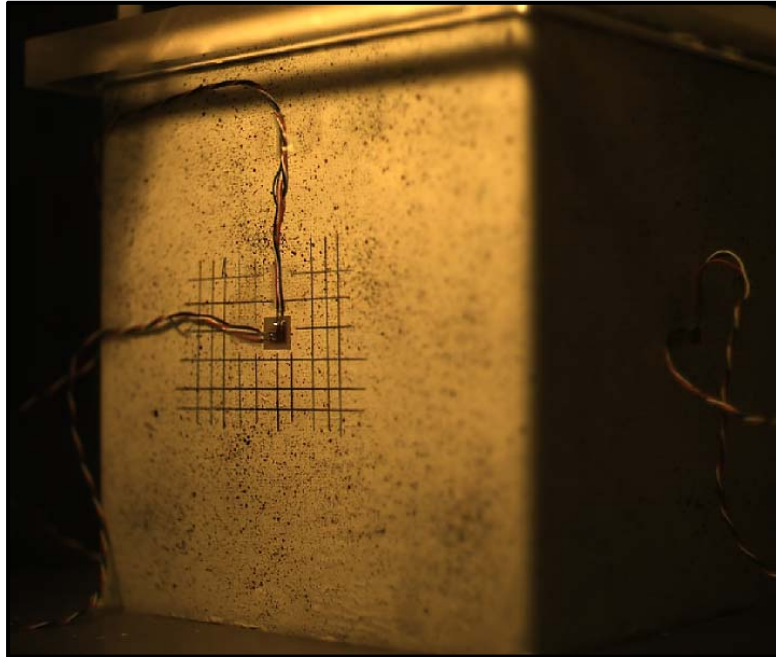
Figure 71.   High-Speed Camera Image of Back Side.

b.   *Top-Down*

The high-speed video from directly above the structure provided insight into how the sides of the structure interacted after the impact. An image from the high-speed video is shown in Figure 72. In all cases, the deformation progressed from the front face around the structure to the back face. The structural response was the same for each case; as the front face deformed inward, the sides deformed outward, and the back side deformed outward. After their initial deformation, all of the sides oscillated and the magnitude of their motion decayed over time. While the general behavior was the same, there were some obvious differences between the various fill levels. In the low fill cases, the magnitudes of the deformation on all sides were less noticeable than that of the high fill cases. The fluid motion was also greater in the high fill cases, except for the 100% case

70

due to the lack of free surface. There was an apparent difference in the behavior on the left and right sides for low fill and high fill cases. At the low fill conditions, the maximum outward deformation on the left and right sides occurred closer to the front side, about 1/4 of the length of the side. At the high fill conditions, the maximum outward deformation was in the center, about 1/2 of the length of the side. The mid fill condition was in between them.
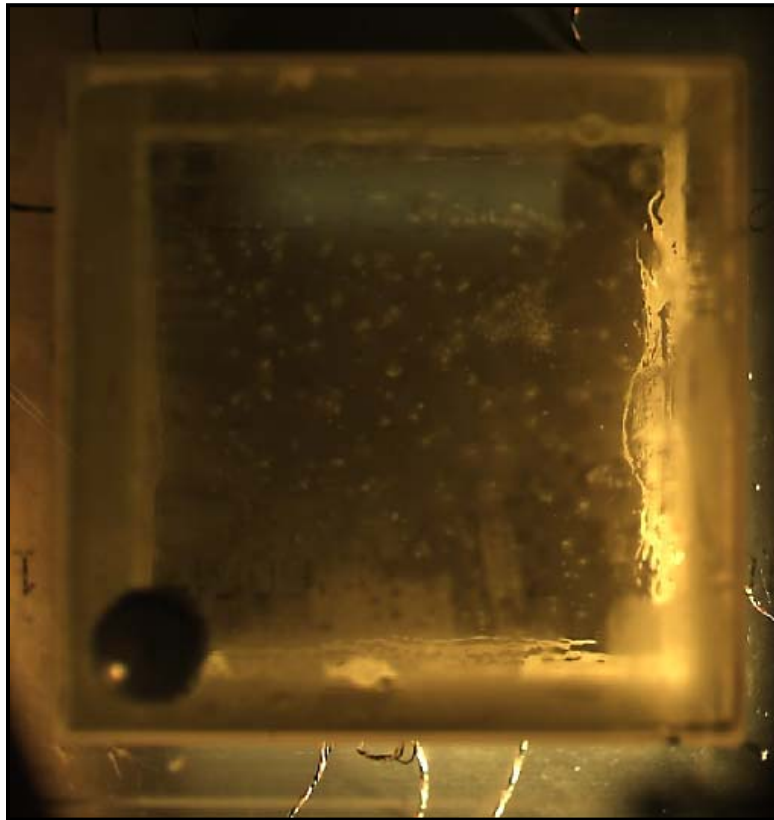
Figure 72.   High-Speed Camera Image of Top (25% fill).

C.   FREQUENCY ANALYSIS

In order to better understand the mode shapes as well as the bifurcation present on the back side at the mid fill level, a Fast Fourier Transform (FFT) was performed on the strain data.

In both the low fill and high fill cases there was a dominant (largest magnitude) frequency present. As the fill level was increased, the dominant frequency decreased. The

strain frequency plot for the back side at 25% fill is shown in Figure 73, and the strain frequency plot for the back side at 75% fill is shown in Figure 74. These plots are representative of the frequency plots for each side and fill level. Although the frequency plot differed slightly between the front, left, right, and back sides, the dominant frequencies were similar. As the back side was the area of interest for this analysis, the frequency trend for the composite structure as the fill level was increased is shown in Figure 75. The lowest dominant frequency of the structure decreased through the low fill and mid fill cases and then plateaued across the high fill cases. This demonstrated a non-linear trend. For the 25 degree and 45 degree impacts, there was a difference in the frequencies at 25% fill and 50% fill, in which the higher impact velocity increased the frequency. This difference was attributed to the influence of sloshing in the higher velocity impact. The lowest dominant frequencies for the various fill levels are listed in Table 7.
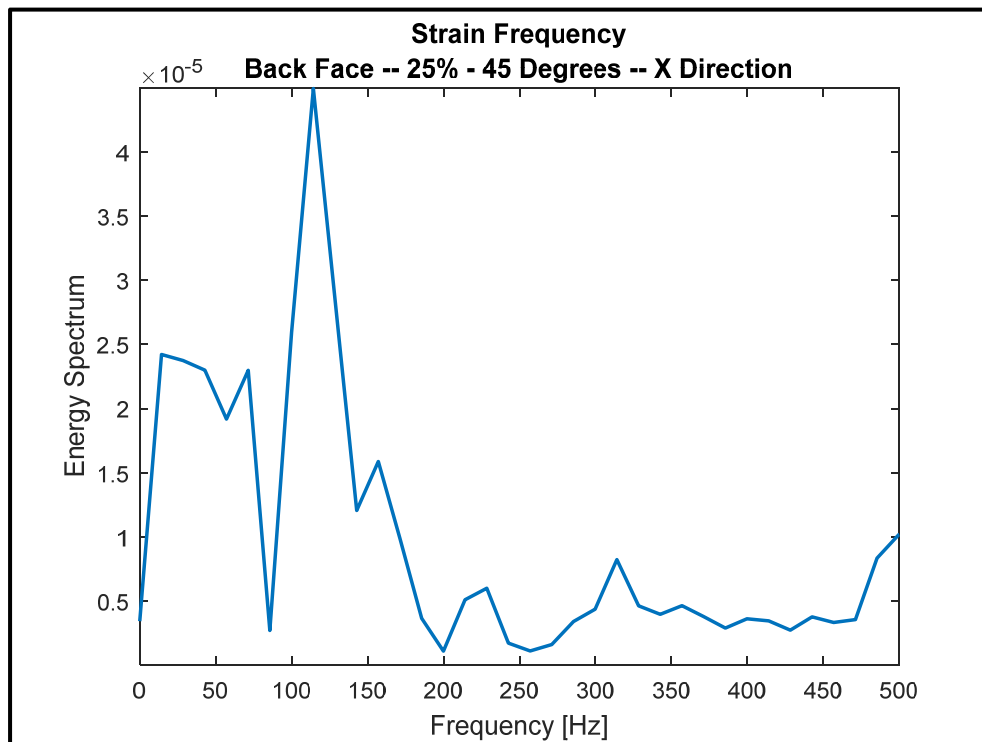
Figure 73.   Strain Frequency Spectrum for 25% Fill.
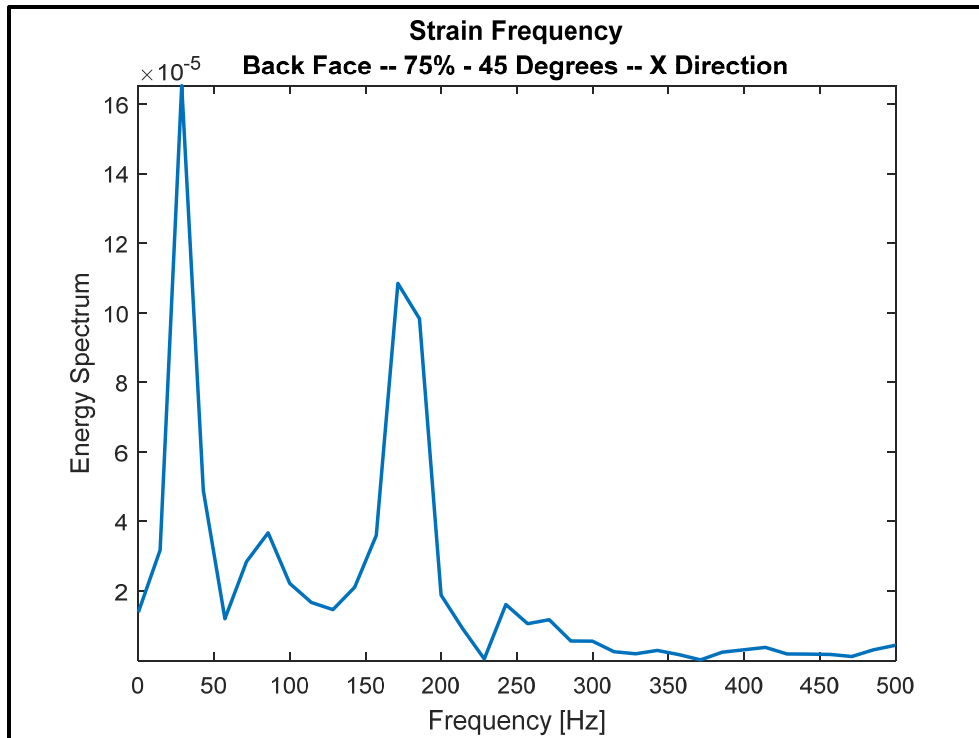
Figure 74.   Strain Frequency Spectrum for 75% Fill.
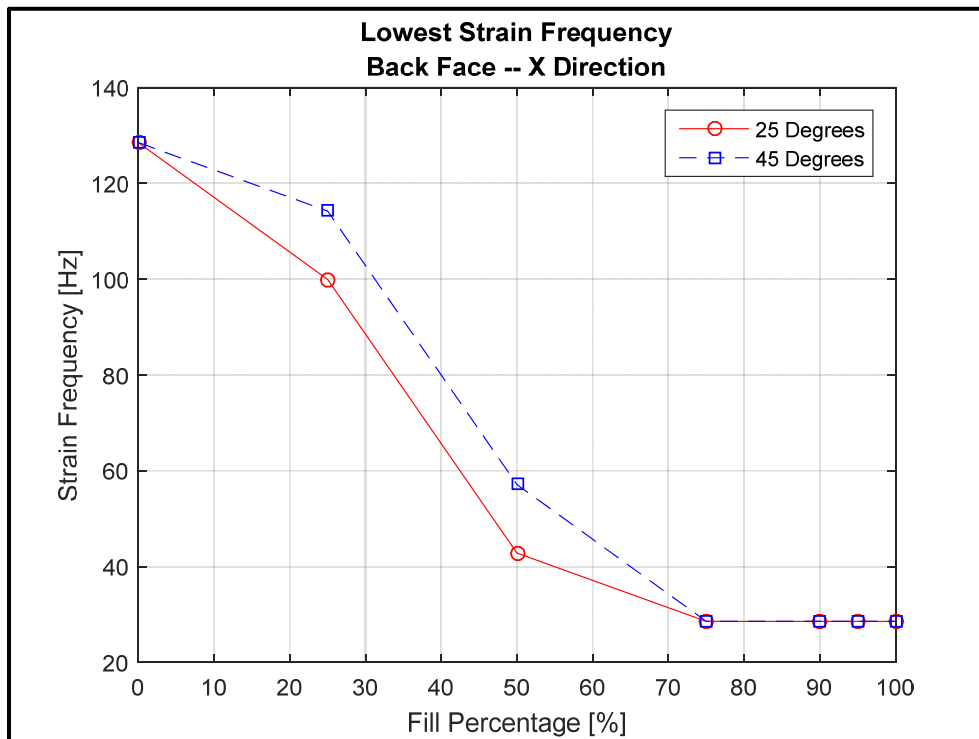
Figure 75.   Strain Frequency of the Back Side Across the Fill Levels.

Table 7.   Lowest Strain Frequency on the Back Side for Fill Levels.

Fill Level	25° Lowest Frequency [Hz]	45° Lowest Frequency [Hz]
0%	128.5	128.5
25%	99.94	114.2
50%	42.83	57.11
75%	28.56	28.56
90%	28.56	28.56
95%	28.56	28.56
100%	28.56	28.56

The frequency plot of the mid fill case, shown in Figure 76, provided clarity to the bifurcation phenomenon that was noticed among the strain on the back side. There were two frequencies that were competing in this condition. Although only two tests are plotted, they are indicative of the 18 tests that were conducted at 50% fill. Half of the tests followed the pattern of "A" and half of the tests followed the pattern of "B." These labels match those in Figure 69 (above). They show that in the case where there is a strong peak at 57.11 Hz ("B"), the maximum strain occurs on the second major peak in compression. In the case where there are equal peaks at 57.11 Hz and 185.6 Hz ("A"), the maximum strain occurs on the first major peak in tension. The frequency that was present in the back side determined that deformation mode shape and the time at which the maximum strain occurred.
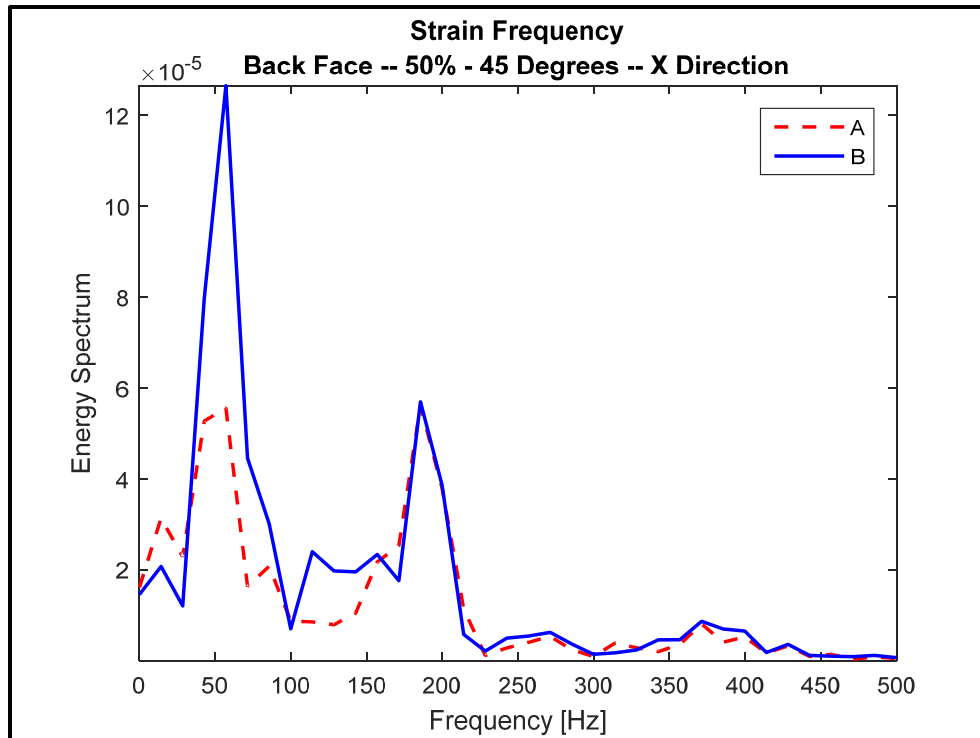
Figure 76.   Strain Frequency Spectrum for 50% Fill.

The final area examined with the frequency analysis was the effect of a baffle on the structural response. There was only one fill level whose frequency at the back side was affected by the addition of a baffle. At 25% fill, both baffles reduced the lowest dominant frequency from 114.2 Hz to 99.94 Hz. This reduction matched the frequency that was present in the 25 degree drop angle. Similar to the difference in the frequencies for the 25% fill and 50% fill for the two drop angles, the reduction with the baffles was attributed to a reduction in sloshing in the fluid. The frequency trend across the various fill levels for the cases with and without a baffle is shown in Figure 77.
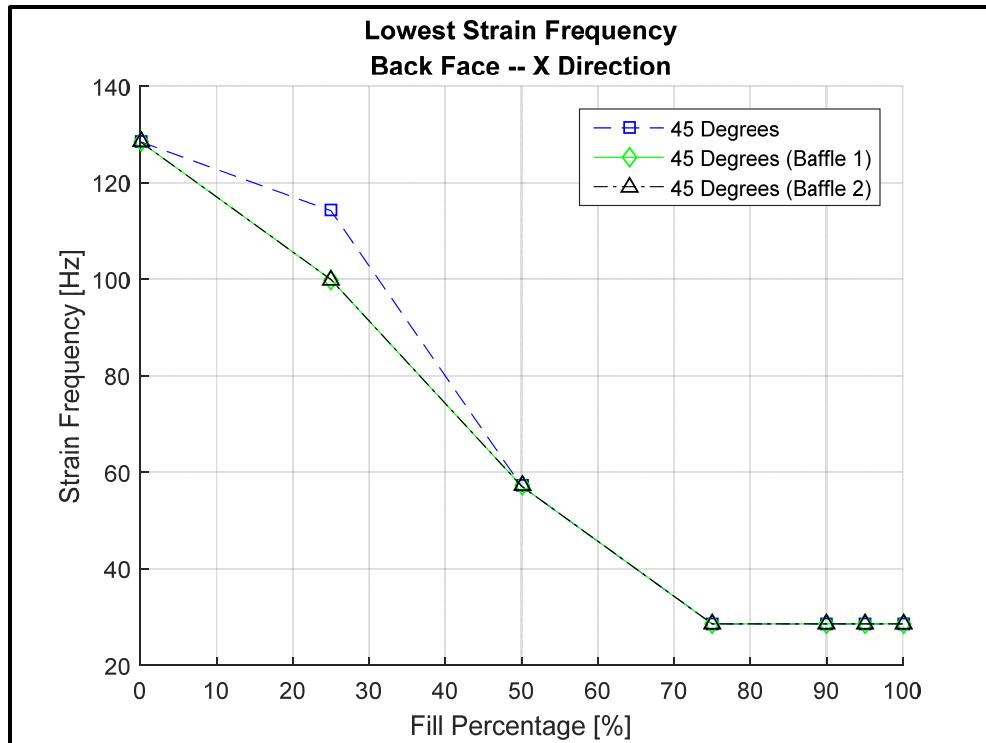
Figure 77.   Strain Frequency Trend for the Back Side across the
Fill Levels (baffles).

IV. CONCLUSIONS AND RECOMMENDATIONS

A. CONCLUSIONS

An experiment was designed and conducted to study the effects of fluid-structure interaction on a fluid-filled composite structure subjected to a low velocity impact. The fluid level was varied incrementally and two different impact velocities were tested. Baffles were also added to the structure to analyze the effects. FSI had a significant impact on the behavior of the structural response of the composite.

The force measured for each impact velocity increased as the fluid level was increased. For both impact velocities, the low fill cases had approximately the same measured force and the high fill cases had the same measured force. The mid fill case was in between them. The impact forces of the 45 degree drop angle were approximately twice those of the 25 degree drop angle. On the front side, in the mid fill and high fill cases there were multiple contacts between the impactor and structure before the impactor rebounded.

The strain response of the composite structure varied with the fluid fill level. On the front side, the structure was initially in tension for the low fill cases and in compression for the mid fill and high fill cases. The maximum strain occurred in compression for all cases except for the full (100%) condition, in which the maximum strain was in tension. As the fill level was increased, the absolute maximum strain also increased. The maximum strain on the front side occurred between 75% fill and 95% fill.

The strain response on the left and right sides were very similar and also varied with the fill level, with the maximum strain magnitude generally increasing as the fill level increased. For both the left and right sides, the maximum strain occurred in tension for all fill levels. The trend of the maximum strain decreased from 0% fill to 25% fill, followed an increase to 75% fill. There was a slight decrease at 90% fill, but the remaining high fill levels showed an increase in strain magnitude. The full (100%) case was the maximum for both sides.

The strain response on the back side showed the most interesting behavior. Similar to the left and right sides, the maximum strain occurred in tension for all fill levels. As the fill level increased, the maximum strain decreased in the low fill cases and mid fill case. The strain increased greatly through the high fill cases with the maximum strain occurring at 95% fill. The amount of time to the maximum strain was also greater in the high fill cases. The mid fill case showed a bifurcation phenomenon in which there were two competing responses. In one response, the maximum strain occurred in tension and in the other, it occurred in compression.

An analysis of the strain frequency showed that the lowest dominant frequency decreased as the fill level increased. There were differences among the two impact velocities in the lower fill cases and mid fill case. On the back side the bifurcation was made clear with the two competing responses showing different frequencies. Where there were differences in frequencies, it was apparent that sloshing was a major contributor.

The effect of a baffle on the front surface was greater than the back surface, especially in the high fill cases. Baffle 1 was more effective in lowering the maximum strain on the front side while Baffle 2 was more effective on the back side. In the case of the bifurcation at 50% fill, Baffle 2 successfully eliminated the phenomenon. Overall, Baffle 2 was considered more effective than Baffle 1 in reducing FSI in the composite structure.

In conclusion, FSI had a large effect on the structural response of the composite and should be given adequate consideration in the design process for composite structures containing fluid.

B.   RECOMMENDATIONS

For continued analysis and study of this topic, additional tests could be conducted to provide more information about the full field response of the structure. With additional strain gages or digital image correlation equipment the full field stress, strain, and deformation could be more accurately characterized. Additionally, the impact location and angle could be varied to determine how they affect the response of the structure.

These results could then be compared with ongoing numerical modelling to verify the structural response.

THIS PAGE INTENTIONALLY LEFT BLANK

APPENDIX. DATA ACQUISITION DETAILS

A. STRAIN GAGE WIRING

The strain gage wire leads were connected to the NI-9945 screw terminal adaptor as shown in Figure 78. The wire leads are described in Table 8.

Figure 78.   Strain Gage Wire Leads into NI-9945 Screw Terminal Adaptor.

Table 8.   Strain Gage Wire Lead Terminal Connections.

Terminal Number	Wire Lead Color	Wire Lead Name
0	Red	Positive
1	White	Negative
2	Black	Ground

B. LOAD CELL WIRING

The load cell wire leads were connected to the NI-9949 screw terminal adaptor as shown in Figure 79. The wire leads are described in Table 9.
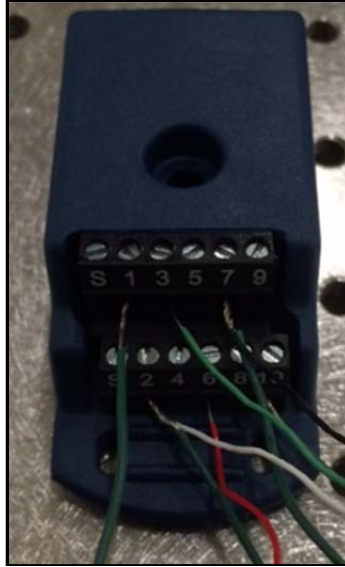
Figure 79.   Load Cell Wire Leads into NI-9949 Terminal Screw Adaptor.

Table 9.   Load Cell Wire Lead Terminal Connections.

Terminal Number	Wire Lead Color	Wire Lead Name
1	Dark green	Jumper (to 2)
2	Dark green	Jumper (to 1)
2	White	(+) Output
3	Light green	(-) Output
6	Red	(+) Excitation
7	Dark green	Jumper (to 10)
7	Black	(-) Excitation
10	Dark green	Jumper (to 7)

C.   LABVIEW SETTINGS

The LabVIEW software was configured to accept simultaneous data acquisition inputs from the strain gages and load cell. The data acquisition was continuous and the maximum achievable sample rate set in order capture the short duration response of the composite structure after impact. The data acquisition settings are listed in Table 10.

Table 10.   LabVIEW Data Acquisition Settings.

Strain Setup	Signal Input Range Max	1 m
	Signal Input Range Min	-1 m
	Scaled Units	Strain
	Gage Factor	2.15
	Gage Resistance	350 ohm
	Vex Source	Internal
	Vex Value (V)	2.5
	Strain Configuration	Quarter Bridge I
	Lead Resistance	0
Force (Bridge) Setup	Signal Input Range Max	500
	Signal Input Range Min	0
	Scaled Units	Pounds
	Bridge Type	Full Bridge
	Vex Source	Internal
	Vex Value (V)	2.5
	Bridge Resistance	350 ohm
Timing Settings	Acquisition Mode	Continuous Samples
	Samples to Read	1500
	Rate (Hz)	30000

D.   HIGH-SPEED CAMERA SETTINGS

The complete list of camera settings used during all high-speed video is shown in Table 11.

Table 11.   High-Speed Camera Settings.

Frame Rate	1000 fps
Shutter Speed	200 μsec
Trigger	50%
Image Size	1280 x 1024

THIS PAGE INTENTIONALLY LEFT BLANK

LIST OF REFERENCES

[1]   Z. Aslan, R. Karakuzu, and B. Okutan, "The response of laminated composite plates under low-velocity impact loading," *Composite Structures*, vol. 53, pp 119–127, Oct. 2002.

[2]   Y. W. Kwon, "Study of fluid effects on dynamics of composite structures," *ASME Journal of Pressure Vessel Technology*, vol. 133, pp 031301–6, Jun. 2011.

[3]   MH-60L Blackhawk Walkaround. (n.d.). ARC Air. [Online]. Available: http://www.aircraftresourcecenter.com/awa01/301–400/awa338-MH-60L/00.shtm.

[4]   S.W. Kim, E.H. Kim, M.-S. Jeong, and I. Lee, "Damage evaluation and strain monitoring for composite cylinders using tin-coated FBG sensors under low-velocity impacts," *Composites Part B*, vol. 74, pp. 13–22, Jan. 2015.

[5]   M. Violette, "Fluid Structure Interaction Effect on Sandwich Composites," M.S. thesis, Department of Mechanical and Aerospace Engineering, Naval Postgraduate School, 2011.

[6]   R. Conner, "Fluid Structure Interaction Effects on Composites Under Low Velocity Impact," M.S. thesis, Department of Mechanical and Aerospace Engineering, Naval Postgraduate School, 2012.

[7]   R. McCrillis, "Dynamic Failure of Sandwich Beams with Fluid-Structure Interaction Under Impact Loading," M.S. thesis, Department of Mechanical and Aerospace Engineering, Naval Postgraduate School, 2010.

[8]   R. D. Firouz-Abadi, H. Haddadpour, and M.A. Kouchakzadeh, "Free vibrations of composite tanks partially filled with fluid," *Thin-Walled Structures*, vol.47, pp 1567–1574, Jul. 2009.

[9]   S. Rebouillat and D. Liksonov, "Fluid-structure interaction in partially filled liquid containers: A comparative review of numerical approaches," *Computers and Fluids*, vol. 39, pp 739–746, Jan. 2010.

[10]   H. M. Koh, J. K. Kim, and J. H. Park, "Fluid-structure interaction analysis of 3-D rectangular tanks by a variationally coupled BEM-FEM and comparison with test results," *Earthquake Engineering and Structural Dynamics*, vol. 27, pp. 109–124, Feb. 1998.

[11]   M. Eswaran, U. K. Saha, and D. Mairy, "Effect of baffles on a partially filled cubic tank: Numerical simulation and experimental validation," *Computers and Structures*, vol. 87, pp. 198–205, Dec. 2008.

[12]   F. Ince, H. S. Turkmen, Z. Mecitoglu, N. Uludag, I. Durgun, E. Altinok, and H. Orenel, "A numerical and experimental study on the impact behavior of box structures," *Procedia Engineering*, vol. 10, pp 1736–1741, 2011.

[13]   J. A. Artero-Guerrero, J. Pernas-Sanchez, J. Lopez-Puente, and D. Varas, "On the influence of filling level in CFRP aircraft fuel tank subjected to high velocity impacts," *Composite Structures*, vol. 107, pp. 570–577, Sep. 2014.

[14]   J. A. Artero-Guerrero, J. Pernas-Sanchez, J. Lopez-Puente, D. Varas, "Numerical analysis of CFRP fluid-filled tubes subjected to high-velocity impact," *Composite Structures*, vol. 96, pp. 286–297, Oct. 2012.

[15]   D. Varas, R. Zaera, and J. Lopez-Puente, "Experimental study of CFRP fluid-filled tubes subjected to high-velocity impact," *Composite Structures*, vol. 93, pp. 2598–2609, May. 2011.

[16]   Pro-Set Inc., Technical Data, M1002 / M2046 Toughened Laminating Epoxy, Bay City, MI: Pro-Set Inc., FEB, 2014.

[17]   D. Miller, "Glass Fiber Resin Composites and Components at Arctic Temperatures," M.S. thesis, Department of Mechanical and Aerospace Engineering, Naval Postgraduate School, 2015.

[18]   F. Mustapha, A. Shahrjerdi, N.W. Sim, "Finite element validation on adhesive joint for composite fuselage model," *Journal of the Brazilian Society of Mechanical Sciences and Engineering*, vol.XXXIV, No.1, pp. 69–74, 2012.

[19]   Fibre Glast Learning Center. (n.d.). Fibre Glast Developments Corporation. [Online]. Available: http://www.fibreglast.com/category/Learning_Center.

[20]   T. Ponshock, "Design and Analysis of an Experimental Setup for Determining the Burst Strength and Material Properties of Hollow Cylinders," M.S. thesis, Department of Mechanical and Aerospace Engineering, Naval Postgraduate School, 2015.

[21]   Lateral Excitation Shaker Stand. (n.d.). The Modal Shop. [Online]. Available: http://www.modalshop.com/excitation/Shaker-Stand?ID=22.

[22]   RS4000 Tuned Damped Top Performance Optical Tables. (n.d.). Newport Corporation. [Online]. Available: http://www.newport.com/RS4000-Tuned-Damped-Top-Performance-Optical-Tables/436017/1033/info.aspx.

[23]   S-2000 Stabilizer Pneumatic Vibration Isolators with Automatic Re-Leveling. (n.d.). Newport Corporation. [Online]. Available: http://www.newport.com/S-2000-Stabilizer-Pneumatic-Vibration-Isolators-w/844255/1033/info.aspx.

[24]   Metal Hemispheres. (n.d.). Sharpe Products. [Online]. Available: http://www.sharpeproducts.com/store/hemispheres.

THIS PAGE INTENTIONALLY LEFT BLANK

INITIAL DISTRIBUTION LIST

1.   Defense Technical Information Center
        Ft. Belvoir, Virginia

2.   Dudley Knox Library
        Naval Postgraduate School
        Monterey, California